UNIVERSITÀ DEGLI STUDI DI PADOVA

Dipartimento di Fisica e Astronomia "Galileo Galilei"

Master's Degree in Physics

Final Dissertation

Conformational phase transitions in models of magnetic polymers

Thesis supervisor

Prof. Enzo Orlandini

Thesis co-supervisor

Prof. Emanuele Locatelli

Candidate

Alberto Raiola

Academic Year 2023/2024

Abstract

Magnetic polymers, where each monomer carries a magnetic moment or spin, are a class of interacting polymers that have recently received attention from the polymer and statistical mechanics community. The reason is at least twofold:

1. they have several applications in Materials Science, in information and communication technology, in sound absorption, in biomedical engineering and in drug delivery;
2. from the statistical mechanics perspective, they are nice examples of interacting systems where the entropy of the polymer substrate and the interaction energy between magnetic spins can give rise to rich equilibrium phase diagrams and non-standard critical phenomena.

Moreover, in the last few years they have been successfully employed in the study of the chromatin folding. Chromatin is a giant polymer located in the cellular nucleus. Its monomers are the nucleosomes, made of a DNA filament twisted around a protein called histone. When an histonic marker (named also epigenetic markers) attaches to an histone, it induces a local modification of the chromatin. Magnetic polymer models are used to understand how the interplay between chromatin (the polymer) folding and epigenetic landscape (the spins) can contribute to shaping the genome organization in the nuclei.

In this thesis, we extended previously investigated models of Ising or Potts-like magnetic polymers to the case in which the underlying magnetic system can, if embedded on a regular lattice, display multicritical behaviours. In particular, we considered the Blume-Emery-Griffiths model where vacancies (i.e. sites with no magnetic moment) are considered. On a regular square lattice, the Blume-Emery-Griffiths model displays a tricritical point between a critical line and line of first-order phase transition. Using mean-field approximations and Monte Carlo simulations, we looked at how the equilibrium phase diagram and the corresponding phase transitions of a lattice polymer model can be shaped by the magnetic interactions, exploring, in particular, the role of the tricritical point on the configurational properties of the polymeric substrate. Strikingly, a mean-field compact disordered phase emerges, that was previously obtained only by driving the system out of equilibrium or by including an overall attractive contribution.

Contents

Chapter 1

Introduction to magnetic polymers

1.1 Polymers

1.1.1 Polymer models

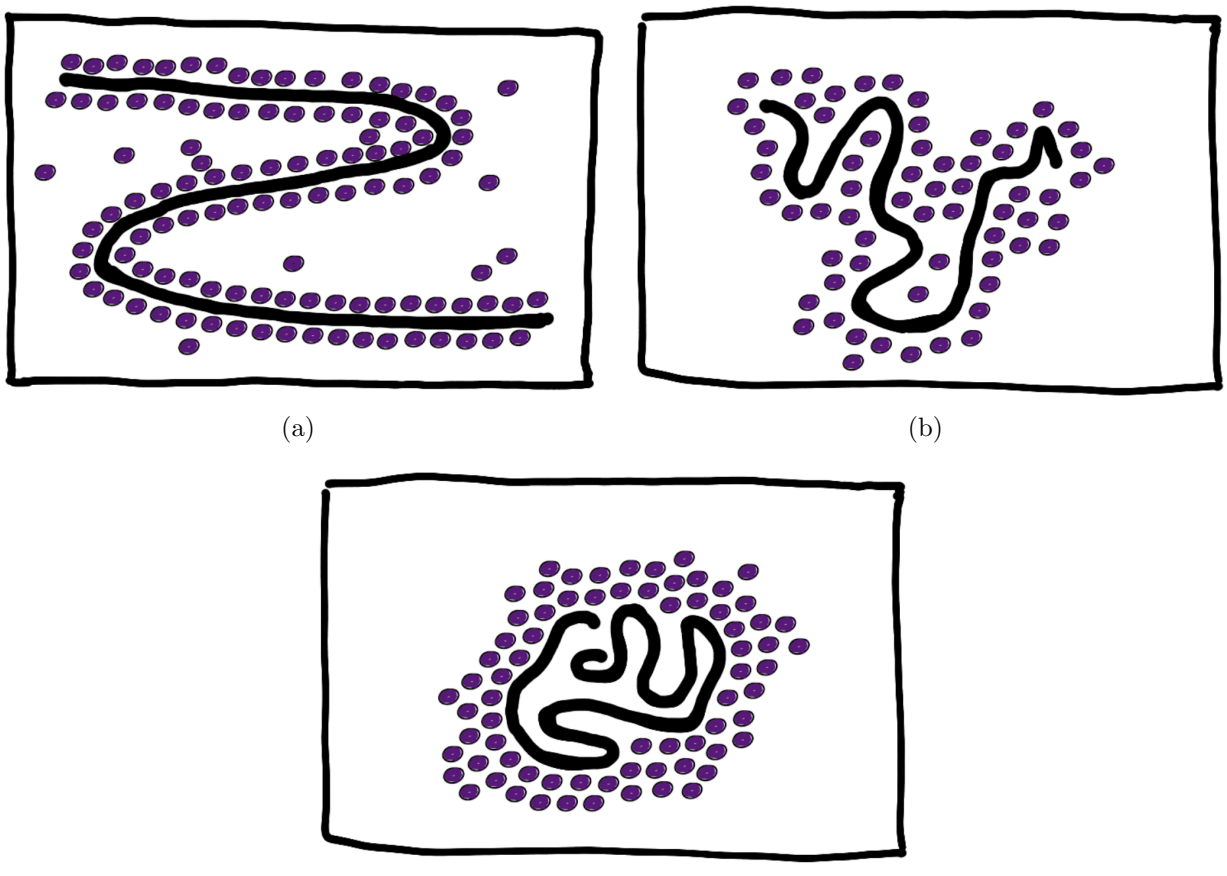

(a) (b) (c)

Figure 1.1: The black line represents the polymer; purple circles correspond to the solvent molecules. (a): in a good solvent the monomers like more the solvent molecules than the other monomers. Thus, it assumes an open, swollen conformation. (b): a polymer immersed in a solvent at the so called θ-point behaves as an ideal coil. The attraction among monomers exactly balances the steric repulsion. (c): in a poor solvent the attraction among monomers is stronger than the hard-core repulsion. The coil is therefore collapsed.

A polymer is a molecule composed of many repeated subunits named monomers. A large variety of such molecules can be find in biological systems: proteins are polymers whose monomer units are the amino acids; nucleic acids (DNA and RNA) are sequences of nucleotides and polysaccharides are long-chain polymeric carbohydrates composed of monosaccharide units.
The physics of such systems is determined by the interplay between the interactions among monomers (inter-polymer interactions) and the effect of the solvent in which the molecules are immersed (see Refs. [1], [2]). An important quantity in this context is the excluded volume per monomer v, a volume inaccessible to other particles because of the presence of a monomer. Thanks to this concept, it is possible to identify three possible regimes:

- If the attraction between monomers is weaker than the steric repulsion between monomers, the excluded volume v is positive and the polymer swells. This corresponds to a *good solvent*: the interaction between solvent molecules and monomers are energetically favorable (see Figure 1.1(a), left);
- If the attraction between monomers just balances the effect of the steric repulsion, the excluded volume vanishes and the chain will adopt a nearly ideal conformation. This correspond to the so called θ-point (see Figure 1.1(b), center);
- If the attraction between monomers is stronger than the steric repulsion, the excluded volume is negative and the polymer collapses. This corresponds to a *poor solvent* (see Figure 1.1(c), right).

Since in an ideal chain excluded volume interactions between monomers are neglected, one can build relatively simple models of ideal polymers, such as the freely jointed chain model, where bonds between monomers have a fixed length and the directions of the different bonds are not correlated. However, it is difficult, in general, to approach real (i.e. non ideal) polymers theoretically because one has to consider all the possible interactions among monomers, including bonds and torsion angles.
In this work we focus on lattice models, where an N-monomers polymer can be mapped on a $(N-1)$-steps walk defined on a lattice of volume V (i.e. whose number of sites is V). The polymer density ρ is defined as $\rho = N/V$. The advantages of using such an approach are its simplicity and the possibility of easily study the equilibrium steady state of the system.
A first attempt of modeling a polymer on a lattice whose coordination number is z is to consider a $(N-1)$ - steps random walk (RW): starting from a lattice site, the next step is determined by selecting randomly one of the neighboring sites (i.e. with probability $1/z$), regardless of whether the site is occupied by another monomer or not. In general, this model is not a good model for non-ideal polymers because it does not take into account repulsive interactions among monomers, induced for instance by steric effects or by the chemical bonds. On the other hand, it can be used to model a polymer in a θ solvent. A more realistic extension of the RW is the so-called self-avoiding walk (SAW), a path on a lattice where a site can be occupied by only one monomer; as such, the path can never cross itself (in Figure 1.2 a RW and a SAW are shown). Given a SAW γ, its adjacency matrix $\Lambda^{\gamma}_{i,j}$ is defined as follows:

$$\Lambda^{\gamma}_{i,j} = \begin{cases} 1 & \text{if } i,j \in \gamma \text{ are nearest neighbors} \\ 0 & \text{otherwise} \end{cases} \tag{1.1}$$

This object allows us to determine the nearest neighbors of a given site and thus to write the interaction terms among monomers in the Hamiltonian of the magnetic polymer model.
Let us consider an $N-1$ steps SAW on a lattice with V sites. We are interested in estimating the number of such walks $\mathcal{Z}_{SAW}$ in the thermodynamic limit ($N \to \infty$ and $V \to \infty$ such shat $\rho = N/V$ remains finite). An exact answer to this problem is actually still an open problem

and only estimates are possible. Heuristically, we can write:

$$\mathcal{Z}_{SAW} = \frac{N!}{(V-N)!}\left(\frac{z}{V}\right)^{N-1}. \tag{1.2}$$

The first factor is the number of ways we can pick N different lattice sites from the total number V. In general they will be far away from each other and do not describe a walk. For this reason we correct this number by inserting the second factor: only the first bead has actually V possible choices, while the remaining ones must be chosen among the z first neighbors. Finally, exploiting the Stirling approximation for the factorials:

$$\log(n!) \approx n\log n - n \tag{1.3}$$

the number of walks can be rewritten as:

$$\mathcal{Z}_{SAW} = \left(\frac{z}{e}\right)^{N} \exp\left(-V(1-\rho)\log(1-\rho)\right) \tag{1.4}$$

Given a SAW γ of N steps on a volume V, other quantities that we will encounter in the following (see the Appendix A) are:

$$\sum_{i,j\in\gamma}(\Lambda^{\gamma}_{i,j})^{-1} \quad \text{and} \quad \sum_{i,j\in\gamma}\Lambda^{\gamma}_{i,j} \tag{1.5}$$

An easy estimation of this quantity can be obtained restricting ourselves to the SAWs that are almost space filling such as, for example, the subset of Hamiltonian walks. An Hamiltonian walk is a path that visits each vertex of a lattice embedded in a volume V exactly once and have been used to study equilibrium properties of highly compact polymers (see Ref. [3]). For an Hamiltonian walk, the adjacency matrix of the SAW Λ takes the same form of the adjacency matrix of the underlying lattice, characterized by the coordination number z. Since our polymer has a density $\rho = N/V$ the expected number of nearest neighbors for each lattice site is $\approx z\rho$, thus:

$$\sum_{i,j}\Lambda^{\gamma}_{i,j} \approx N\rho z \tag{1.6}$$

and

$$\sum_{i,j}(\Lambda^{\gamma}_{i,j})^{-1} \approx \frac{N}{\rho z}. \tag{1.7}$$

In the following it will be useful to find how many $(N-1)$-steps SAWs can be drawn on a finite volume V.

1.1.2 Interacting SAW

The previous concepts can be easily used to to model the behavior of homopolymers (i.e. polymers whose monomers are identical) in a solution. The polymer is modeled as a $(N-1)$-steps SAW γ on a volume V lattice whose coordination number is z. The interaction among two nearest neighbor monomers i and j is supposed to be attractive:

$$\mathcal{I}(i,j) = -\epsilon\Lambda^{\gamma}_{i,j} \qquad \epsilon > 0. \tag{1.8}$$

The Hamiltonian of such a model is:

$$\mathcal{H} = \frac{1}{2}\sum_{i,j}\mathcal{I}(i,j) = -\frac{\epsilon}{2}\sum_{i,j}\Lambda^{\gamma}_{i,j} \tag{1.9}$$

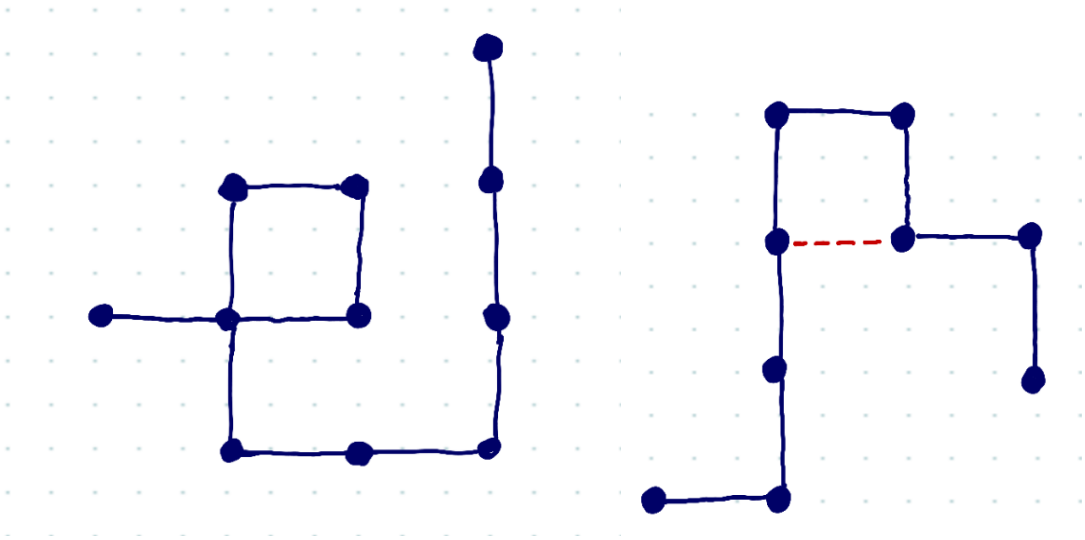

(a) (b)

Figure 1.2: Examples of walks. (a): In this picture a RW on a square lattice is shown. Such kind of walks can cross themselves. (b): An example of self avoiding walk (SAW). It does not cross itself. Red dashed line represents the self avoidance.

The thermodynamics of this model is obtained applying equilibrium statistical mechanics. The partition function is defined as:

$$\mathcal{Z}(\beta,\rho;\epsilon)=\sum_{\gamma\in\mathrm{SAW}}\exp\left(\frac{\beta\epsilon}{2}\sum_{i,j}\Lambda_{i,j}^{\gamma}\right) \tag{1.10}$$

where $\beta=1/T$ is the inverse temperature. Applying the relations Eqs. (1.2) and (1.6) we find:

$$\mathcal{Z}_{MF}(\beta,\rho;\epsilon)=\left(\frac{z}{e}\right)^{N}\exp\left(-V(1-\rho)\log(1-\rho)+\frac{\beta\epsilon}{2}Nz\rho\right) \tag{1.11}$$

The free energy density is:

$$f(\beta,\rho;\epsilon)=-\frac{1}{N\beta}\log\mathcal{Z}_{MF}(\beta,\rho,\epsilon)= \tag{1.12}$$

$$=-\frac{1}{\beta}\log\left(\frac{z}{e}\right)+\frac{1}{\beta}\frac{1-\rho}{\rho}\log(1-\rho)-\frac{\epsilon z}{2}\rho. \tag{1.13}$$

From the minimum free energy principle we can obtain the equilibrium polymer density ρ in different temperature regimes. Let us Taylor expand Eq. (1.13) around $\rho=0$:

$$\frac{1-\rho}{\rho}\log(1-\rho)=-1+\frac{\rho}{2}+\frac{\rho^2}{6}+\frac{\rho^3}{12}+\dots \tag{1.14}$$

$$f(\beta,\rho;\epsilon)=f_0(\beta,\epsilon)+\left(\frac{1}{2\beta}-\frac{\epsilon z}{2}\right)\rho+\frac{1}{6\beta}\rho^2+\dots. \tag{1.15}$$

where

$$f_0(\beta;\epsilon)=-\frac{1}{\beta}\log\left(\frac{z}{e}\right)-\frac{1}{\beta} \tag{1.16}$$

Since the coefficients in front of the higher powers of ρ are positive, we expand till the second order. Eq. (1.15) is quadratic in ρ therefore the position of the minimum depends on the sign

of the linear coefficient:

$$\rho^* = 0 \qquad \text{if} \qquad \epsilon z\beta \leq 1 \tag{1.17}$$

$$\rho^* = \frac{3}{2}(\epsilon z\beta - 1) \qquad \text{if} \qquad \epsilon z\beta > 1 \tag{1.18}$$

Therefore, when $\beta < 1/z\epsilon$ the polymer is in a swollen phase; when $\beta > 1/z\epsilon$ the polymer collapses in a compact phase. Since the function $\rho^*(T)$ is continuous at the critical temperature $\beta^* = 1/z\epsilon$, this simple model predicts a continuous swollen-disordered phase transition. In Figure 1.3 the temperature trend of the equilibrium density has been computed numerically from Eq. (1.13). In this figure the coordination number z and the magnitude of the attractive interaction ϵ have been set to unity. The observed critical $\beta^* = 1$ corresponds with the result obtained previously.

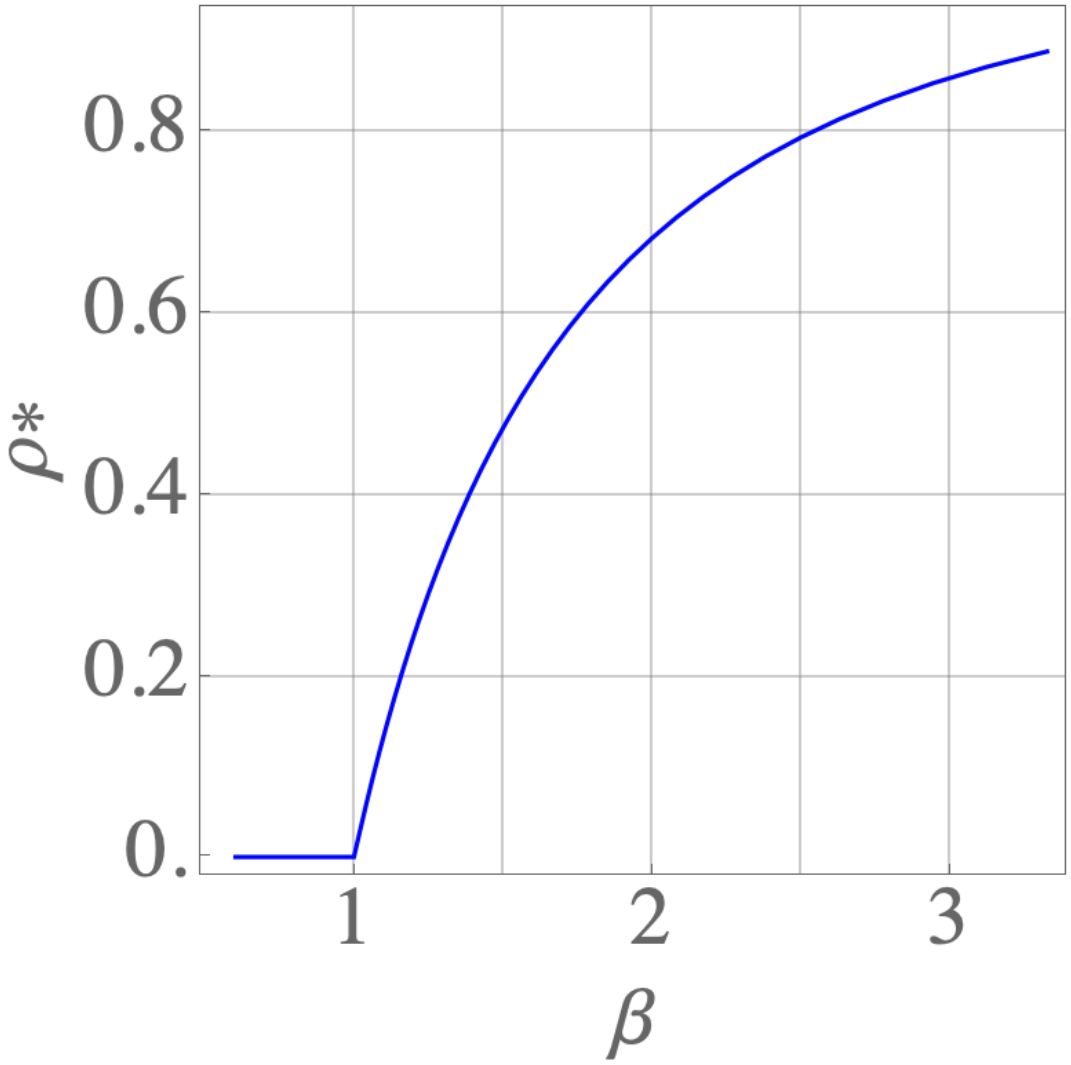

Figure 1.3: Temperature behavior of the equilibrium polymer density $\rho*$, computed numerically from Eq. (1.13). In this plot $z = \epsilon = 1$. The critical value of inverse temperature is $\beta^* = 1$ which corresponds to the result obtained Taylor expanding the free energy density.

1.1.3 Virial expansion

Starting from the free energy density we can compute the osmotic pressure Π. Its thermodynamic definition is:

$$\Pi = -\frac{\partial f}{\partial(1/\rho)} = \rho^2 \frac{\partial f}{\partial \rho} \tag{1.19}$$

By Taylor expanding it around $\rho = 0$, the osmotic pressure can be rewritten as a virial expansion:

$$\Pi(\rho) = B_1\rho + B_2\rho^2 + B_3\rho^3 + \dots, \tag{1.20}$$

where B_i is the i-th virial coefficient. These coefficients can be determined starting from experimental data or can arise from a theoretical model.
In general the i-th virial coefficient is a "measure" of the i-bodies interaction. In particular, the first virial coefficient is connected to the ideal behavior (and corresponds to the Van't Hoff osmotic pressure) and the second virial coefficient give us information about the excluded volume. When the second virial coefficient is positive, the excluded volume is finite and positive meaning that the interaction between the monomers is, overall, repulsive. In this situation the polymer is expected to swell (it corresponds to Figure 1.1(a)). When B_2 is negative, the opposite occurs: attraction dominates and the polymer is expected to collapse (Figure 1.1(c) right). The ideal behavior is recovered when $B_2 = 0$ (the θ point, Figure 1.1(b)).
The virial expansion helps us to study the properties of the swollen-disordered phase transition. For the interacting SAW model described before, the second and third virial coefficients corresponds to the coefficients in front of the linear and squared term:

$$B_2(\beta, \epsilon) = \frac{1}{\beta}\left(\frac{1}{2} - \frac{\beta\epsilon z}{2}\right) \tag{1.21}$$

$$B_i(\beta) = \frac{1}{\beta}\frac{1}{(i+1)} \qquad i > 2 \tag{1.22}$$

and from B_2 we can derive a measure of the excluded volume v:

$$v = \beta B_2(\beta, \epsilon) = \left(\frac{1}{2} - \frac{\beta\epsilon z}{2}\right) \tag{1.23}$$

Therefore:

$$v > 0 \qquad \text{if} \quad \beta < \beta^* \tag{1.24}$$

$$v = 0 \qquad \text{if} \quad \beta = \beta^* \tag{1.25}$$

$$v < 0 \qquad \text{if} \quad \beta > \beta^* \tag{1.26}$$

Varying the temperature, it is possible to go from a good solvent to a bad solvent. The temperature $\theta = 1/\beta^*$ such that $v(\theta) = B_2(\theta) = 0$ is called theta temperature, that marks the onset of the swollen-disordered phase transition.

1.1.4 Magnetic polymers

In physics many models have been defined in order to study the magnetic properties of materials. In general, given a lattice, a magnetic model consists in assigning a spin variable S_i to each site i and defining how they interact among each others. In order to define a magnetic polymer model, we need to take into account the topology of a SAW on the lattice: this can be done by means of the adjacency matrix as defined in Eq. (1.1). The Hamiltonian of the model is:

$$\mathcal{H}_\gamma(\{S\};\{\psi\}) = \frac{1}{2}\sum_{i,j=1}^{N} \Lambda_{i,j}^{\gamma} \mathcal{J}(S_i, S_j; \psi), \tag{1.27}$$

where $\gamma \in$ SAW is a self avoiding walk, $\mathcal{J}(S_i, S_j; \psi)$ defines the interaction among the two spins S_i and S_j belonging to the walk γ and $\{\psi\}$ is a set of parameters characterizing the interaction (in a ferromagnetic Ising - like interaction, the parameter is the exchange energy). In this way two spin variables may interact only if they below to the SAW and if they are nearest neighbors. Starting from the Hamiltonian of the model one can theoretically compute the partition function of the system:

$$\mathcal{Z}(\rho, \{\mathcal{O}\}, \beta; \{\psi\}) = \sum_{\gamma \in \text{SAW}} \sum_{\{S\}} \exp\left(-\beta \mathcal{H}_\gamma(\{S\}; \{\psi\})\right). \tag{1.28}$$

$\beta = 1/T$ is the inverse temperature, $\{\mathcal{O}\}$ is a set of n order parameters that, together with ρ, characterize the macroscopic state of the system (in this work the maximum number of order parameters, that will be considered, is $n = 2$ for the BEG model). From it we can derive the whole thermodynamics of the system, including the free energy density:

$$f(\rho, \{\mathcal{O}\}, \beta; \{\psi\}) = -\frac{1}{\beta N} \log \mathcal{Z}(\beta, \rho, \{\psi\}) \tag{1.29}$$

where log is the natural logarithm. As well known, this is practically impossible because of the complexity of the model. However, working in the mean field approximation, this task is generally achievable.
The phase diagram of such a model can be numerically derived by solving a system of mean field equations:

$$\frac{\partial f}{\partial \rho} = 0 \qquad \frac{\partial f}{\partial \mathcal{O}_j} = 0 \quad j = 1, \ldots, n. \tag{1.30}$$

varying the inverse temperature β and the parameters $\{\psi\}$ of the model.
From the previous mean field equations it is possible to write the order parameters $\mathcal{O}_j(\rho)$ in terms of the polymer density. By plugging these relations in Eq. (1.29) and expanding it around $\rho = 0$ it is possible to derive the virial coefficients and study in detail the swollen-disordered transition.
The phases a magnetic polymer system can display are typically characterized by the polymer density ρ and the magnetization per spin m:

$$m = \frac{1}{N} \sum_{i=1}^{N} S_i = \langle S_i \rangle. \tag{1.31}$$

It is possible to define four phases on the basis of the values of the previous two order parameters:

- *Compact ordered* (CO): $\rho > 0$, $m > 0$;
- *Compact disordered* (CD): $\rho > 0$, $m \simeq 0$;
- *Swollen ordered* (SO): $\rho \simeq 0$, $m > 0$;
- *Swollen disordered* (SD): $\rho \simeq 0$, $m \simeq 0$;

A SO phase is typically never observed.

1.2 Ising magnetic polymer

In this section we summarize the results of Ref. [4] about an Ising magnetic polymer. The procedure detailed before will be applied to study the conformational phase transitions of an Ising magnetic polymer, whose monomers interact ferromagnetically according to the Hamiltonian of the Ising model.

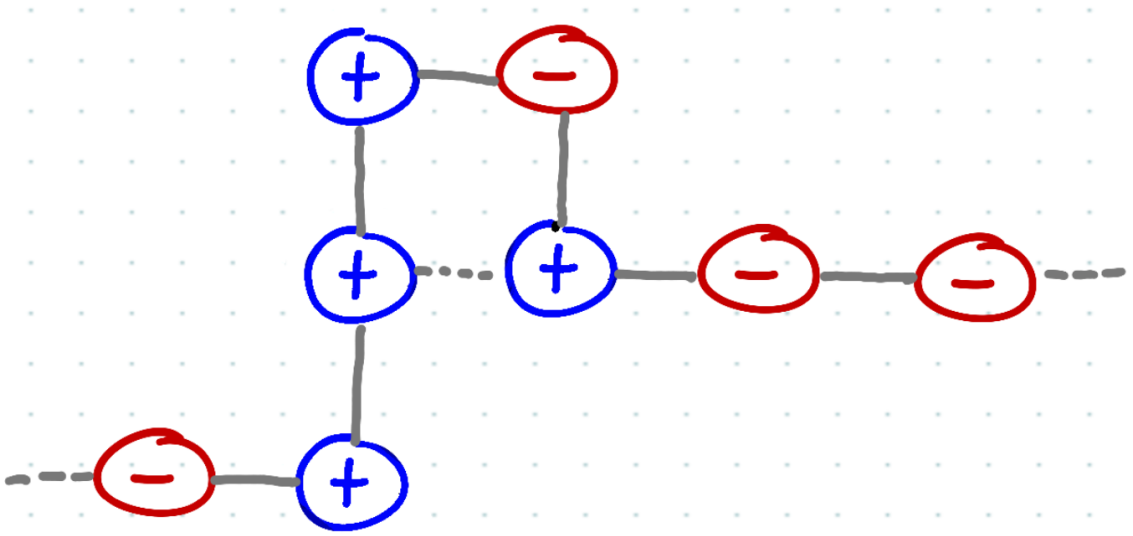

Figure 1.4: An Ising magnetic polymer is modeled as a SAW. All the monomers carry a spin variable and nearest neighbor monomers interact ferromagnetically following Eq. (1.33). Straight black lines represents the walk, the dotted line represent a ferromagnetic interaction among two non consecutive beads.

1.2.1 Hamiltonian of the system

Let the spin variables S_i assume the two following values: $S_i \in \{-1, 1\}$. The interaction energy among a couple of spin variables belonging to the SAW is defined as:

$$\mathcal{J}(S_i, S_j) = -JS_iS_j \tag{1.32}$$

where J is the exchange energy. Moreover, let us add an homogeneous magnetic field $h_i \equiv h$ for each site i of the SAW. Given a SAW γ, the Hamiltonian of the system becomes:

$$\mathcal{H}_\gamma(\{S\}; J, h) = -\frac{J}{2}\sum_{i,j=1}^{N} S_i\Lambda^\gamma_{i,j}S_j - h\sum_{i=1}^{N} S_i \tag{1.33}$$

In Figure 1.4 a sketch of Ising magnetic SAW is shown. Straight black lines represents the walk, the dotted line represent a ferromagnetic interaction among two non consecutive beads.

1.2.2 Mean field theory

The partition function of the system is obtained summing the Boltzmann factors with respect to all the possible SAWs and all the possible spin configurations:

$$\mathcal{Z} = \sum_{\gamma\in\text{SAW}}\sum_{\{S\}} \exp\left(\frac{\beta J}{2}\sum_{i,j} S_i\Lambda^\gamma_{i,j}S_j + \beta h\sum_i S_i\right) \tag{1.34}$$

All the calculation regarding this partition function are reported in the Appendix, section 1. Let us summarize here the procedure:

- We perform an Hubbard - Stratonovich transformation in order to decouple the two spin variables in the first term inside the exponential. In order to do this we must introduce a set of local fields $\{\phi_i\}$, one for each monomer, and to integrate over them;
- It is then possible to perform the summation on the spin variables;

- Finally, an homogenous saddle point approximation allows us to find a mean field partition function of the system. The sum on the SAWs is performed applying Eq. (1.2) and Eq. (1.7).

The mean field partition function is:

$$\mathcal{Z} \approx A \left(\frac{z}{e}\right)^N \exp\left(-V(1-\rho)\log(1-\rho) - \frac{N\phi^2}{2\beta\rho z J} + \sum_{i=1}^{N} \log(2\cosh(\phi+\beta h))\right), \tag{1.35}$$

where A is a constant factor. The mean field free energy density of this model is:

$$f(\phi,\rho,\beta;J,h) = +\frac{\phi^2}{2\rho\beta^2 Jz} - \frac{1}{\beta}\log\frac{z}{e} + \frac{1}{\beta}\frac{1-\rho}{\rho}\log(1-\rho) - \frac{1}{\beta}\log(2\cosh(\phi+\beta h)), \tag{1.36}$$

Which corresponds to Eq. (11) of Ref. [4]. Finally, we can derive the expression of the average magnetization per spin m:

$$m = \langle S_i \rangle = -\frac{\partial f}{\partial h} = \tanh(\phi+\beta h). \tag{1.37}$$

1.2.3 Phase diagrams and virial expansion

The mean field equations arising from Eq. (1.36) are:

$$\frac{\partial f}{\partial \phi} = 0 \tag{1.38}$$

$$\frac{\partial f}{\partial \rho} = 0 \tag{1.39}$$

which correspond to:

$$\frac{\phi^2}{2\beta Jz} = -\rho - \log(1-\rho) \tag{1.40}$$

$$\phi = \beta Jz\rho\tanh(\phi+\beta h) = \beta Jz\rho m \tag{1.41}$$

Solving numerically the previous system of equations it is possible to draw the mean field phase diagram of the Ising polymer. In general, given a couple (T,h) of values of temperature and magnetic field, there could be multiple solutions. The physical one, which ensure thermodynamical stability, is the one which minimizes the free energy density Eq. (1.36). In particular, Eq. (1.41) allows us to link the field ϕ to the average magnetization per spin:

$$\phi = \beta Jz\rho m. \tag{1.42}$$

In Figure 1.5 heat maps of the magnetization per spin m (left panel) and of the polymer density ρ (right panel) are showed on the plane h-T. In these graphs, and in the following ones, the coordination number has been set to $z = 6$ (which corresponds to a three dimensional squared lattice) and the exchange energy is set to $J = 1$. From Figure 1.5 it is possible to identify the presence of a CO and a SD phases. Moreover, the transition between these two phases seems to be discontinuous for low values of h and continuous for large h. No other phase is observed. We can Taylor expand Eq. (1.41) around $\phi = 0$ up to the first order, finding out a relation between the field ϕ and the polymer density ρ:

$$\phi(\rho) \approx \frac{\beta J\rho z\tanh(\beta h)}{\beta J\rho z\tanh^2(\beta h) - \beta J\rho z + 1} \tag{1.43}$$

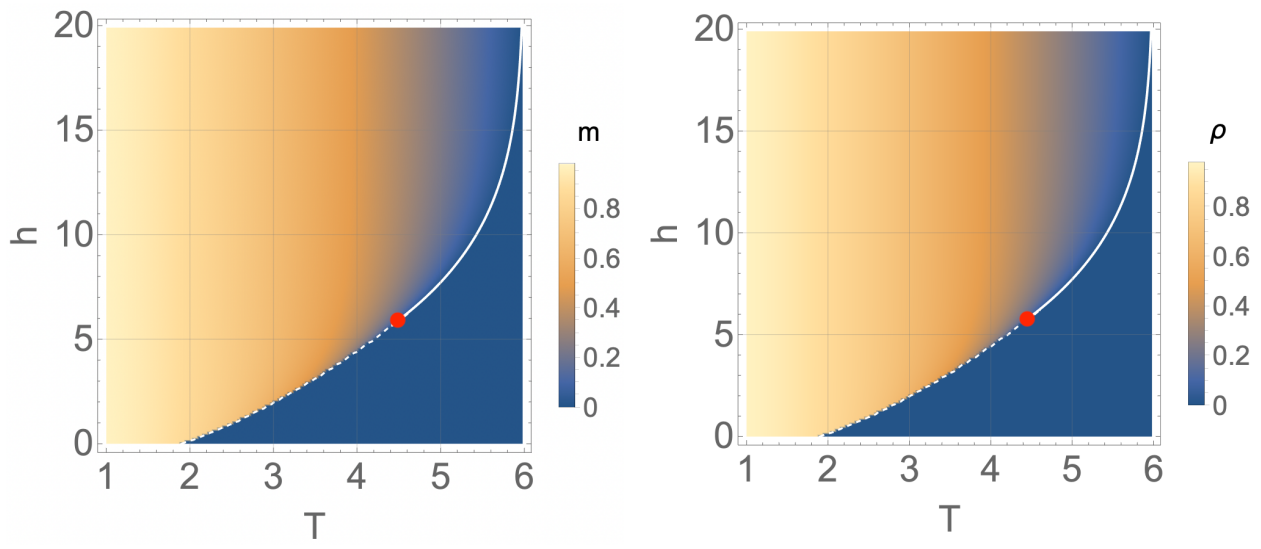

(a) (b)

Figure 1.5: Heat maps computed numerically from the system of equations (1.40) and (1.41). The coordination number has been set to $z = 6$ and the ferromagnetic exchange constant $J = 1$. The white line corresponds to the CO - SD transition. A full and dashed line correspond to a second order and a first order phase transition respectively. The red dot corresponds to the tricritical point G. (a): magnetization m per spin in the h-T plane. (b): polymer density ρ in the plane h-T plane.

Plugging this relation in Eq. (1.36) and Taylor expanding around $\rho \approx 0$ it is possible to derive the virial coefficients:

$$B_2(\beta, J, h) = \frac{\beta(J-2)Jz\tanh^2(\beta h) + 1}{2\beta} \tag{1.44}$$

$$B_3(\beta, J, h) = \frac{1}{3\beta} - \beta J^2(2J-3)z^2\tanh^4(\beta h) + \beta J^2(2J-3)z^2\tanh^2(\beta h) \tag{1.45}$$

Both the coefficients vanish at the multicritical point G (the fourth coefficient is instead positive):

$$G = (T_G, h_G) = \left(\frac{9J}{2}, \frac{9J}{2}\operatorname{arctanh}\frac{\sqrt{3}}{2}\right) = (4.5J, 5.9J) \tag{1.46}$$

Above the critical point, the condition $B_2(\beta, J, h) = 0$ corresponds to the critical θ line, since $B_3(\beta, J, h) > 0$.
In the phase diagrams in Figure 1.5 the transition line between the CO and the SD phases is shown. The continuous line corresponds to the continuous θ transition and has been drawn putting the second virial coefficient to zero. The dashed line, corresponding to a discontinuous phase transition and computed numerically, meets the previous one in the multi critical point G. The swollen - disordered transition when the magnetic field h vanishes occurs at a temperature $T \approx 1.886J$.

Chapter 2

The Blume-Emery-Griffiths model

2.1 Introduction

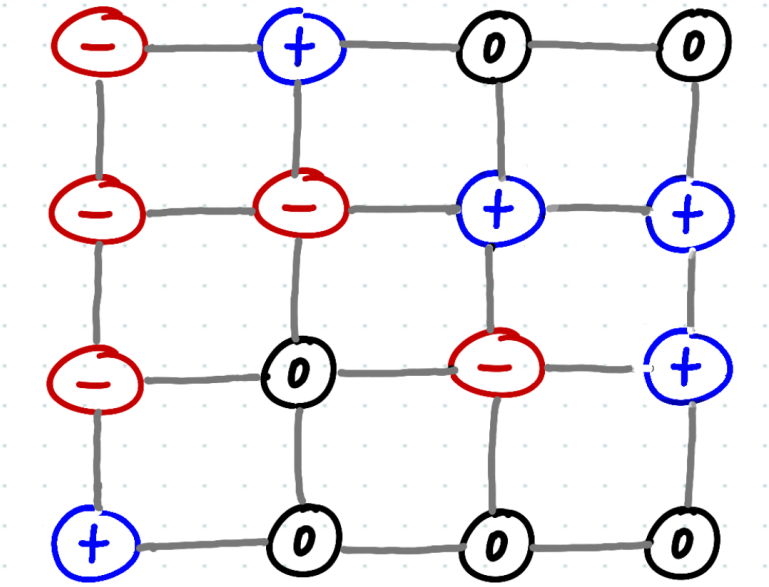

Figure 2.1: A 4×4 square lattice. Each lattice sites carry a spin variable $S_i \in \{0, \pm 1\}$ and their interaction is ruled by Eq. (2.1).

The Blume-Emery-Griffith model (BEG model, see Ref. [5]) was proposed in the 1971 as a lattice model for the fluid-superfluid transition of a binary mixture of He^3 - He^4. In fact, a gas of He^4 is a gas of bosons and ordinarily undergoes a second order phase transition from a non zero to a zero viscosity phase by decreasing the temperature. Such a kind of a transition is of the λ type because of the peculiar λ-shape assumed by the graph of the specific heat around the critical temperature T_λ. By adding to this gas a certain amount of He^3 (fermions), the gas of bosons will be diluted, and therefore the critical properties of such a model are affected.
Experimentally it is observed that above a critical concentration of fermions $x_{tc} \approx 0.67$, the fluid - superfluid transition becomes of the first order. The main feature of the BEG is to reproduce this phenomenon, by predicting the presence of a tricritical point on the phase diagram which separates a line of critical points from a line of first order transitions.
Starting from the Hamiltonian of the model, we derive a mean field theory of this model through an Hubbard - Stratonovich transformation followed by an homogeneous saddle point approximation. From the mean field free energy function it is possible to derive the mean

field equations and thus the phase diagram of this model. Let us consider a lattice whose coordination number is z (for a square lattice defined in d dimension, $z = 2d$). Each lattice site carries a spin variable $S_i \in \{0, \pm 1\}$, where $i = 1, 2, \ldots, N$ and N is the total number of sites (see Figure 2.1). The Hamiltonian of the BEG model is:

$$\mathcal{H}(\{S\}; J, K, \Delta) = \underbrace{-J \sum_{\langle i,j \rangle} S_i S_j}_{\text{ferromagnetic term}} \underbrace{-K \sum_{\langle i,j \rangle} S_i^2 S_j^2 + \Delta \sum_{i=1} S_i^2}_{\text{interaction term}} - \Delta N \tag{2.1}$$

- In terms of Helium isotopes, vacancies represent an He^3 (fermions) while ± 1 spins represent He^4 (bosons);
- Angular brakets $\langle ij \rangle$ are used to indicate a sum on neighboring spins;
- The first term, where $J > 0$ is responsible for the "superfluid" ordering.
- The second ($K \geq 0$ is the strength of the biquadratic interaction) and the third term ($\Delta \propto \mu_3 - \mu_4$, where μ_3 and μ_4 are the chemical potentials of the two helium isotopes) represent the interaction energy between isotopes.
- The last term is the chemical potential term.

In this chapter the BEG model is presented following Ref. [5]. We will analyze in detail the two limiting cases $K = 0$ and $J = 0$ and finally we will discuss three cases with a finite ratio K/J. The derivation of the free energy density for a BEG magnetic polymer is analogous to that for an Ising magnetic polymer: the main differences are reported in the second chapter of the appendix. Their expressions are:

$$\mathcal{Z} = A \left(\frac{z}{e}\right)^N \exp\left(-\frac{N\phi^2}{2\beta z J} - \frac{N\alpha^2}{2\beta z K} + N \log(1 + 2e^{-\beta\Delta + \alpha} \cosh(\phi + \beta h))\right), \tag{2.2}$$

$$f(\beta, \phi, \alpha, \rho) = \frac{1}{2\beta^2 z}\left(\frac{\phi^2}{J} + \frac{\alpha^2}{K}\right) - \frac{1}{\beta} \log(1 + 2e^{-\beta\Delta + \alpha} \cosh(\phi)) - \Delta. \tag{2.3}$$

2.2 K = 0

2.2.1 Mean field free energy

Setting to zero the strength of the biquadratic interaction, the Hamiltonian Eq. (2.1) reduces to:

$$\mathcal{H}_{K=0}(\{S\}; J, \Delta) = -J \sum_{\langle ij \rangle} S_i S_j + \Delta \sum_{i=1}^{N} S_i^2 - \Delta N. \tag{2.4}$$

Notice that in the limit $\Delta \to -\infty$ one should recover the phenomenology of the Ising model because of the absence of vacancies. Following the procedure reported in the section 2 of the appendix, neglecting the biquadratic interaction, the computed mean field partition function and free energy density are respectively:

$$\mathcal{Z}(\phi, \beta; J, \Delta) = \exp\left(-\frac{N\phi^2}{2z\beta J} + N \log\left(1 + 2e^{-\beta\Delta} \cosh(\phi)\right) + \beta\Delta N\right), \tag{2.5}$$

$$f(\phi, \beta; J, \Delta) = -\frac{1}{N\beta} \log Z_N = \frac{\phi^2}{2z\beta^2 J} - \frac{1}{\beta} \log\left(1 + 2e^{-\beta\Delta} \cosh(\phi)\right) - \Delta. \tag{2.6}$$

To characterize the magnetic properties of such model we must compute the average magnetization per spin $m = \langle S_i \rangle$. This task can be performed by introducing in the Hamiltonian a $-h \sum_i S_i$ term; computing the magnetization from its thermodynamic definition:

$$m = -\frac{\partial f}{\partial h} \tag{2.7}$$

and finally sending $h \to 0$. The introduction of this novel term in the Hamiltonian induces the presence of a $+\beta h$ inside the hyperbolic cosine in Eq. (2.6). The result of this computation is:

$$m = \frac{2e^{-\beta\Delta} \sinh \phi}{1 + 2e^{-\beta\Delta} \cosh \phi}. \tag{2.8}$$

Let us compute another interesting thermodynamic variable: the average concentration of vacancies (or of ^{3}He) is defined as $x = 1 - \langle S_i^2 \rangle$:

$$\langle S_i^2 \rangle = \frac{\partial f}{\partial \Delta} + 1 \tag{2.9}$$

$$x = -\frac{\partial}{\partial \Delta} f = 1 - \frac{2e^{-\beta\Delta} \cosh \phi}{1 + 2e^{-\beta\Delta} \cosh \phi} = \frac{1}{1 + 2e^{-\beta\Delta} \cosh \phi}. \tag{2.10}$$

In particular, the concentration of vacancies in the disordered phase is:

$$x(\phi = 0) = \frac{1}{1 + 2e^{-\beta\Delta}} \tag{2.11}$$

and this quantity will be used in what follows in order to characterize the critical properties of the BEG model.

2.2.2 Criticality and tricriticality

In order to study the critical properties of this model we want to Taylor expand the free energy density Eq. (2.6). Because of the $\mathbb{Z}_2$ symmetry of this model we expect to observe only even powers of ϕ in the Taylor expansion of $f(\phi, \beta; \Delta)$ around $\phi = 0$.
The free energy expansions in terms of ϕ is (neglecting terms that do not depend on ϕ, see section 3 of the Appendix for technical details):

$$\begin{aligned} f(\phi, \beta; \Delta) &= \left(\frac{1}{2\beta^2 Jz} - \frac{1}{2\beta\delta} \right) \phi^2 - \frac{1}{8\beta} \left(\frac{1}{3\delta} - \frac{1}{\delta^2} \right) \phi^4 + \frac{1}{48\beta\delta^2} \phi^6 \\ &= a(\beta, \Delta)\phi^2 + b(\beta, \Delta)\phi^4 + c(\beta, \Delta)\phi^6 \end{aligned}$$

where we have defined:

$$\delta = 1 + \frac{e^{\beta\Delta}}{2} \tag{2.12}$$

$$a(\beta, \Delta) = \left(\frac{1}{2\beta^2 Jz} - \frac{1}{2\beta\delta} \right) \tag{2.13}$$

$$b(\beta, \Delta) = -\frac{1}{8\beta} \left(\frac{1}{3\delta} - \frac{1}{\delta^2} \right) \tag{2.14}$$

$$c(\beta, \Delta) = \frac{1}{48\beta\delta^2} \tag{2.15}$$

Notice that $c(\beta, \Delta) > 0$ while instead $a(\beta, \rho, \Delta)$ and $b(\beta, \Delta)$ may change sign.
The critical condition is:

$$\begin{aligned} a(\beta, \Delta) &= 0 \\ b(\beta, \Delta) &> 0, \end{aligned}$$

which leads to:

$$\begin{aligned} \beta J z &= \delta \\ \delta &< 3 \end{aligned}$$

or equivalently to:

$$\begin{aligned} \beta J z &= \frac{1}{1 - x(\phi = 0)} \\ x(\phi = 0) &< 2/3 \end{aligned}$$

Which tell us that on the $T - x$ plane the critical points lay on a straight line. $x(\phi = 0) = 1/(1 + 2e^{-\beta\Delta})$ is the concentration of vacancies in the disordered phase. The tricritical point arises when both the previous coefficients vanish:

$$\begin{aligned} a(\beta, \Delta) &= 0 \\ b(\beta, \Delta) &= 0 \end{aligned}$$

$$\begin{aligned} \beta_{TC} J z &= 3 \\ \delta_{TC} &= 3 \end{aligned}$$

or equivalently:

$$\begin{aligned} \beta_{TC} J z &= 3 \\ x(\phi = 0)_{TC} &= 2/3 \end{aligned}$$

When $\delta > 3$, or equivalently, when $x(\phi = 0) > 2/3$ a first order phase transition is expected. An analytical estimation of the transition temperature and of the boundaries of the coexistence region on the $x - T$ plane, valid in the proximity of the tricritical point, can be achieved by imposing:

$$b^2(\beta, \Delta) = 4a(\beta, \Delta)c(\beta, \Delta).$$

In this way, the two minima of the free energy Taylor expansion have the same height in the graph. For lower temperatures, numerical methods are needed.

2.2.3 Numerical analysis and mean field phase diagrams

The mean field self consistent equation for the ϕ field is:

$$\frac{\partial f}{\partial \phi} = 0 \rightarrow \phi = \beta J z \frac{\sinh \phi}{\frac{e^{\beta\Delta}}{2} + \cosh \phi}. \tag{2.16}$$

It is interesting to notice that from Eqs. (2.8) and (2.16) we can derive a relationship between the field ϕ and the magnetization per spin: $\phi = \beta J z m$.
By solving numerically Eq. (2.16) for ϕ and applying Eq. (2.10) it is possible to derive heat

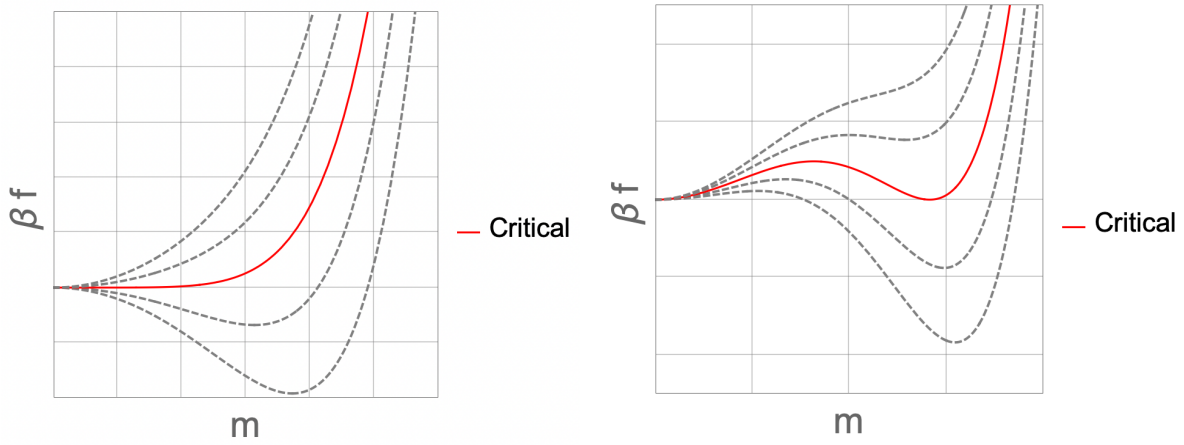

(a) (b)

Figure 2.2: Lines represent the free energy Eq. (2.6) at different values of T; in particular, the full red line corresponds to the free energy computed on the point of the phase diagram where a transition is expected. (a): $x(\phi = 0) = 0.3$ and therefore we expect to observe a continuous phase transition. (b): $x(\phi = 0) = 0.8$ and we observe a first order phase transition.

maps of the magnetization and of the concentration of vacancies in the $\Delta - T$ plane. In Figures 2.3(a) and 2.3(b) such kind of graphs are shown (the coordination number and the ferromagnetic exchange energy have been set respectively to $z = 6$ and $J = 1$). In the first panel, the magnetization per spin m changes smoothly from one to zero across the critical line $\Delta = T \log(2(Jz/T - 1))$ (derived from the definition of δ); the tricritial point is located in $(\Delta_{tc}, T_{tc}) = (4 \log 2J, T_{tc} = 2J)$. For $\Delta_{tc} < \Delta \lesssim 3J$ a discontinuity is observed. From the second panel it is possible to observe that the ordered phase display a lower concentration of vacancies, as expected. It is also possible to derive numerically the boundaries of the coexistence region in the $x - T$ plane (notice that here x is the concentration of vacancies, not just restricted to the disordered phase) by using Eqs. (2.10) and (2.16). In Figure 2.3(c) the phase coexistence region is displayed. An interesting result shown in Ref. [5] is that the slope of the λ line is continuous in intersecting the right boundary of the coexistence region: this result is typical of mean field theories.

2.3 $J = 0$

When the ratio K/J diverges (i.e. $J = 0$), only the interaction energy is present and therefore the magnetization m is equal to zero. The Hamiltonian reduces to:

$$\mathcal{H}_{J=0}(\{S\}; K, \Delta) = -K \sum_{\langle i,j \rangle} S_i^2 S_j^2 + \Delta \sum_{i=1} S_i^2 - \Delta N. \tag{2.17}$$

The mean field partition function and mean field free energy density are respectively:

$$\mathcal{Z}(\alpha, \beta; K, \Delta) = A \left(\frac{z}{e}\right)^N \exp\left(-\frac{N\alpha^2}{2\beta z K} + N \log(1 + 2e^{-\beta\Delta+\alpha})\right), \tag{2.18}$$

$$f(\alpha, \beta; K, \Delta) = \frac{1}{2\beta^2 z}\frac{\alpha^2}{K} - \frac{1}{\beta}\log(1 + 2e^{-\beta\Delta+\alpha}) - \Delta. \tag{2.19}$$

where A is a constant. In this case the average concentration of vacancies x is:

$$x = \frac{1}{1 + 2e^{-\beta\Delta+\alpha}} \tag{2.20}$$

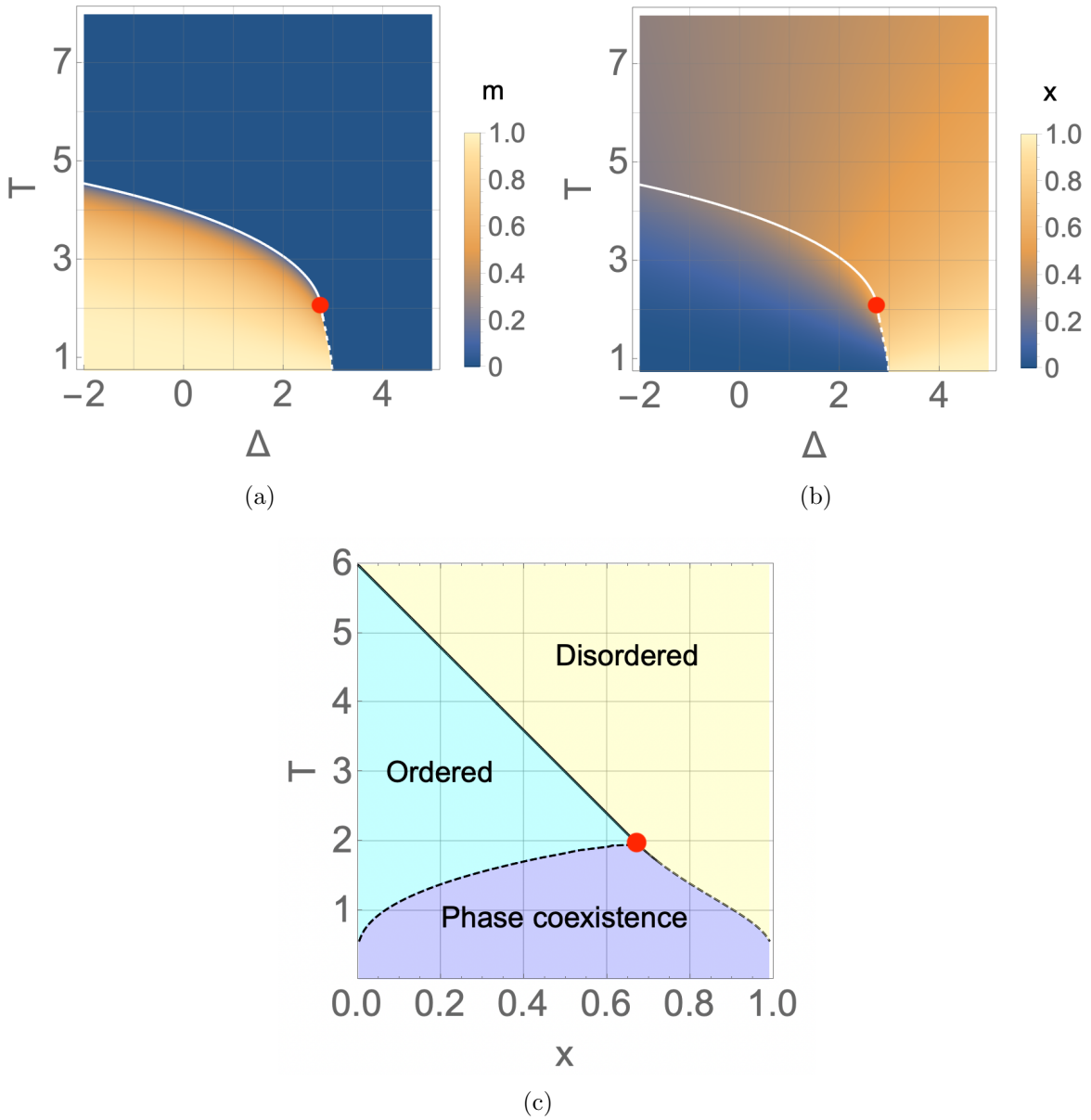

(a) (b)

(c)

Figure 2.3: (a): heat map of the magnetization m on the T - Δ plane. (b): heat map of the average concentration of vacancies x on the T - Δ plane. White lines corresponds to the transition line: a dashed and a full line correspond respectively to a discontinuous and a continuous phase transition. Red point corresponds to the tricritical point. (c): Phase diagram in the T - x plane. Three different regions are distinguishable: an ordered one where the magnetization $m > 0$, a disordered one, where $m = 0$, and a phase coexistence region, where these two phases coexist.

The Taylor expansion of the free energy density around $\alpha = 0$ is given by:

$$f(\alpha, \beta; K, \Delta) = a(\beta, K, \Delta)\alpha^2 + b(\beta, K, \Delta)\alpha^3 + c(\beta, K, \Delta)\alpha^4 \tag{2.21}$$

where:

$$a(\beta, K, \Delta) = \frac{\frac{1}{Kz} - \frac{2\beta e^{\beta\Delta}}{\left(e^{\beta\Delta}+2\right)^2}}{2\beta^2} \tag{2.22}$$

$$b(\beta, K, \Delta) = -\frac{e^{\beta\Delta}\left(e^{\beta\Delta}-2\right)}{3\beta\left(e^{\beta\Delta}+2\right)^3} \tag{2.23}$$

$$c(\beta, K, \Delta) = -\frac{e^{\beta\Delta}\left(-8e^{\beta\Delta}+e^{2\beta\Delta}+4\right)}{12\beta\left(e^{\beta\Delta}+2\right)^4} \tag{2.24}$$

A critical point C is found when $a(\beta, K, \Delta) = b(\beta, K, \Delta) = 0$ and $c(\beta, K, \Delta) > 0$: this happens when $T = 1/\beta = 3/2$ and $\exp(\beta\Delta) = 2$ implying $x = 0.5$ (see Figure 2.4). At lower temperatures, the transition is expected to be discontinuous. The heat map is drawn solving numerically the following mean field equation:

$$\frac{\partial f}{\partial \alpha} = \frac{\frac{\alpha}{Kz} - \frac{2e^{\alpha}\beta}{2e^{\alpha}+e^{\beta\Delta}}}{\beta^2} = 0 \tag{2.25}$$

and the binodal curve is numerically computed using Eqs. (2.20) and (2.25).

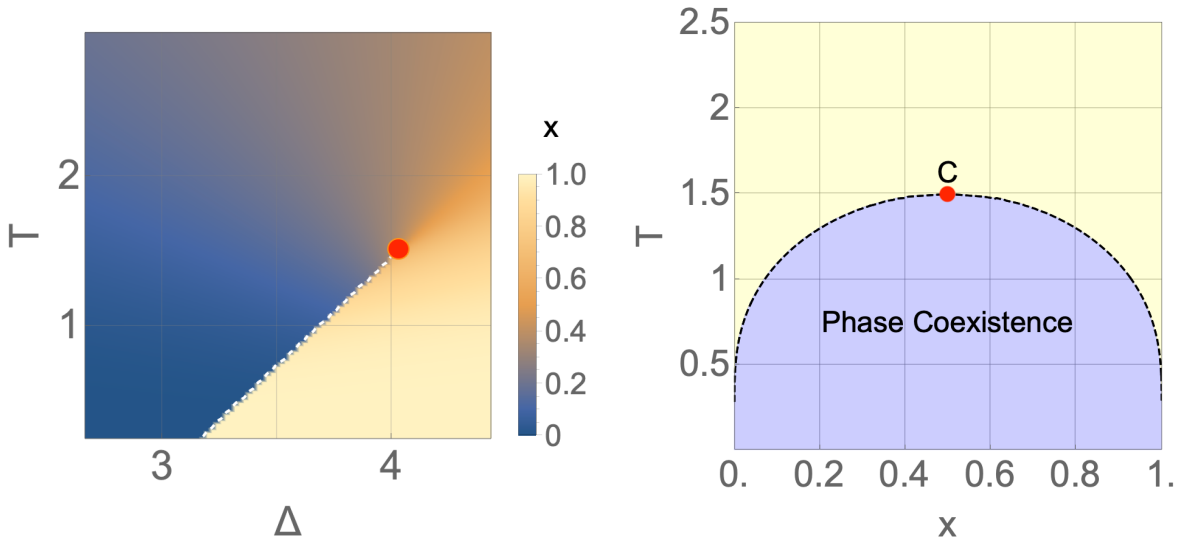

(a) (b)

Figure 2.4: Phase diagrams for the $J = 0$ case. The coordination number and the strength of the biquadratic interaction have been set to $z = 6$ and $K = 1$ respectively. (a): heat map showing the average concentration of vacancies x on the $T - \Delta$ plane. The white dashed line corresponds to a discontinuous phase transition. The red dot position corresponds to the critical point C. (b): phase diagram on the $T - x$ plane. C is the critical point, and below it a discontinuous phase transition separates two phases with different average number of vacancies.

2.4 Intermediate cases

Cases where $0 < K/J < \infty$ are physically relevant because the presence of competing interactions is ubiquitous in physical systems and usually brings a great richness to the phase diagram. Indeed, we see that tricritical points and triple points appear, at different values of the ratio K/J.

The mean field free energy and the mean field partition functions are Eqs. (2.18) and (2.19). The average magnetization per spin $m = \langle S_i \rangle$ and the average concentration of vacancies $x = 1 - \langle S_i^2 \rangle$ are respectively:

$$m = \frac{2e^{-\beta\Delta+\alpha}\sinh(\phi)}{1 + 2e^{-\beta\Delta+\alpha}\cosh(\phi)} \tag{2.26}$$

$$x = \frac{1}{1 + 2e^{-\beta\Delta+\alpha}\cosh(\phi)} \tag{2.27}$$

The phase diagram of such a model can be derived by solving numerically the following mean field equations:

$$\frac{\phi}{\beta J z} - \frac{\sinh(\phi)}{\frac{e^{\beta\Delta-\alpha}}{2} + \cosh(\phi)} = 0 \tag{2.28}$$

$$\frac{\alpha}{\beta K z} - \frac{\cosh(\phi)}{\frac{e^{\beta\Delta-\alpha}}{2} + \cosh(\phi)} = 0 \tag{2.29}$$

This system of mean field equations allows us to link the field ϕ to the the average magnetization per spin and the field α to the average concentration of vacancies:

$$\phi = \beta J z m \tag{2.30}$$

$$\alpha = \beta K z (1 - x) \tag{2.31}$$

It is possible to derive again the position of the tricritical point in terms of the peculiar quantities of this model. Expanding the free energy density in Taylor series around $\phi = 0$ and $\alpha = 0$, it turns out (see Ref. [5]) that the tricritical temperature and the tricritical average concentration of vacancies are:

$$T_{tc} = \frac{1 + 2K/J}{3 + 2K/J} z \qquad x_{tc} = \frac{2}{3 + 2K/J} \tag{2.32}$$

In the following the phase diagrams emerging from the same values of the ratio K/J chosen by the authors of Ref. [5] are studied.

2.4.1 $K/J = 0.16$

A ratio $K/J \gtrsim 0$ causes only quantitative changes from the $K = 0$ case (see Figure 2.5, where $K/J = 0.16$). The tricritical point shifts to a smaller value of x and a larger value of T. For the case of the Figure 2.5, the coordinates of the tricritical point are $(x_{tc}, T_{tc}) \approx (0.60, 2.39)$.

2.4.2 $K/J = 2.88$

As the ratio increases, it is possible to observe features of both the $K = 0$ and the $J = 0$ cases. In particular, this situation is rather peculiar because a tricritical point, a critical point and a triple point appear together in the same phase diagram. See Figure 2.6, in the right panel: the phase coexistence region displays two maxima: the first one is the tricritical point (whose coordinates are $(x_{tc}, T_{tc}) \approx (0.23, 4.63J)$), at the intersection between the λ line, due to the ferromagnetic term in the Hamiltonian; the second one is a new critical point C. A triple point (whose coordinates are approximatively $(x_{tp}, T_{tp}) \approx (0.6, 4.25J)$) is also present, where an ordered and poorly diluted phase coexists together with two disordered and diluted phases.

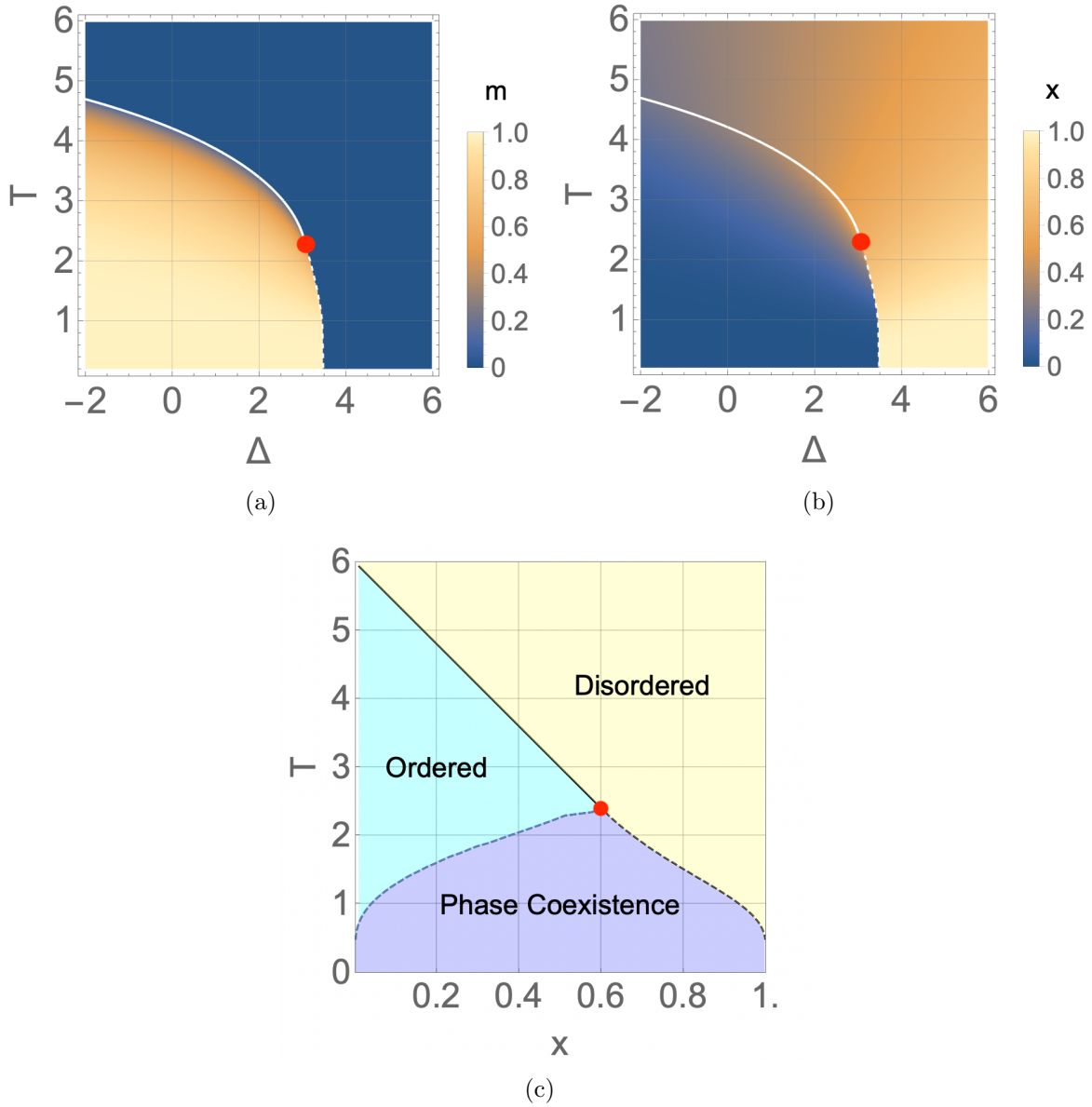

(a) (b)

(c)

Figure 2.5: Phase diagrams for the $K/J = 0.16$ case. (a): heat map showing the magnetization m in the $T - \Delta$ plane. The white dashed and continuous lines correspond to a discontinuous and a full phase transition respectively. The red dot position corresponds to the tricritical point. (b): heat map showing the average concentration of vacancies x on the $T - \Delta$ plane. (c): Phase diagram on the $T - x$ plane. The tricritical point has moved to a lower concentration of vacancies x and an higher temperature with respect to the $K/J = 0$ case of Figure 2.3(c).

2.4.3 $K/J = 3.8$

Increasing again the ratio, the tricritical point moves below the critical point C (see Figure 2.7). Actually, despite appearing on the phase diagram at the coordinates $(x_{tc}, T_{tc}) \approx (0.19, 4.86J)$, the ordered - disordered phase coexistence is metastable with respect to the phase coexistence generated by the interaction. In fact, in Ref. [5], the authors draw a diagram similar to plane on the right of Figure 2.4, where the λ - line merely intersects the boundaries of the phase coexistence region.

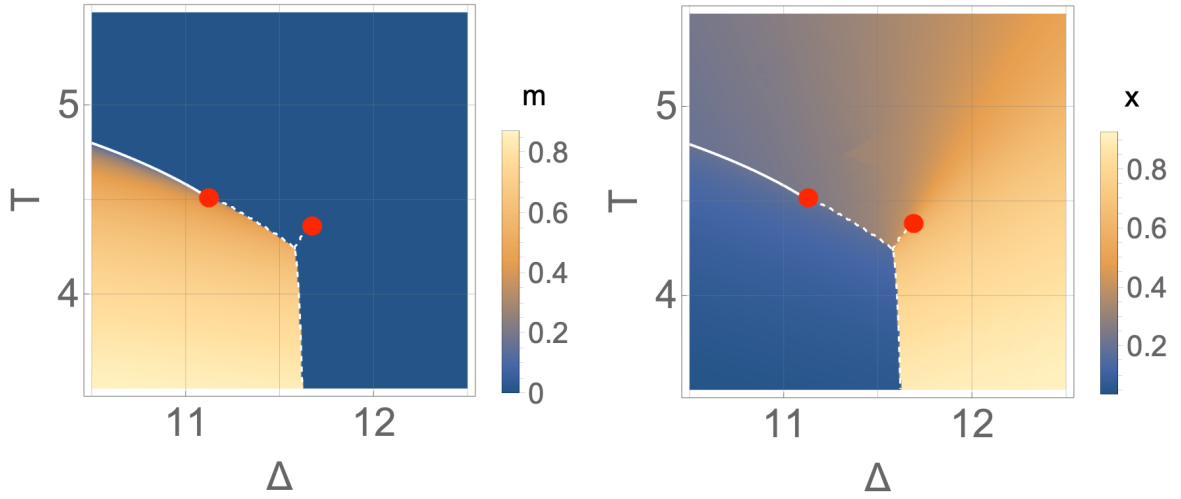

(a)

(b)

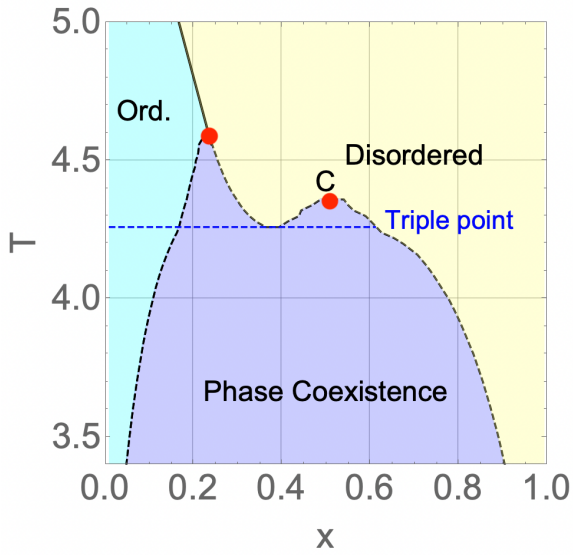

(c)

Figure 2.6: Phase diagrams for the $K/J = 2.88$ case. (a): heat map showing the magnetization m on the $T - \Delta$ plane. The white dashed and full lines correspond to a discontinuous and a continuous phase transition respectively. The red dot corresponds to the critical and tricritical points. (b): heat map showing the average concentration of vacancies x on the $T - \Delta$ plane. (c): Phase diagram on the $T - x$ plane. The triple point has been highlighted with a blue dashed line.

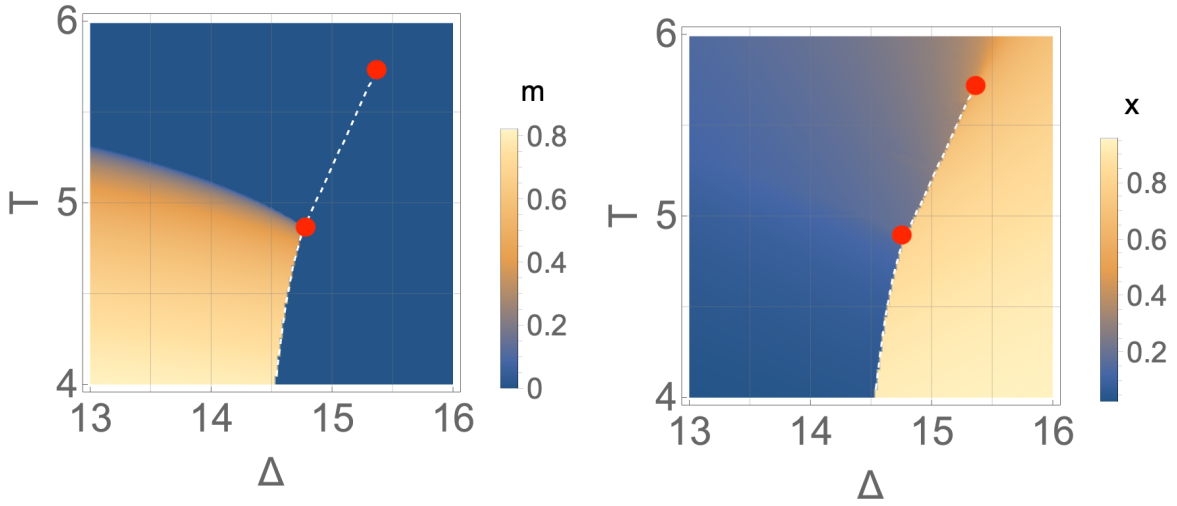

(a) (b)

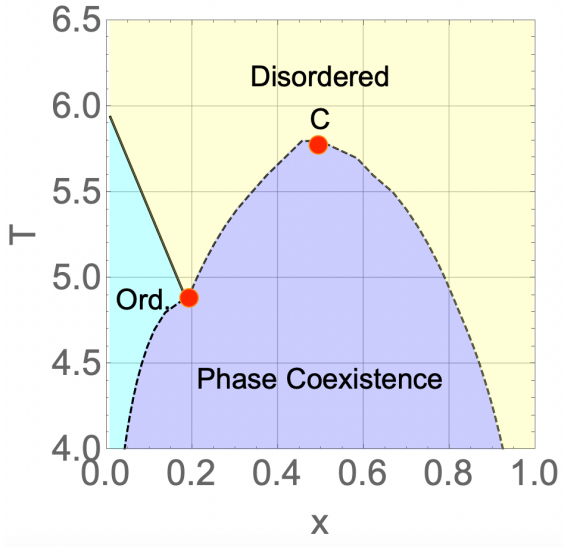

(c)

Figure 2.7: Phase diagrams for the $K/J = 3.8$ case. (a): heat map showing the magnetization m on the $T - \Delta$ plane. The white dashed and full lines correspond to a discontinuous and a continuous phase transition respectively. The red dot corresponds to the critical and tricritical points. (b): heat map showing the average concentration of vacancies x on the $T - \Delta$ plane. (c): Phase diagram on the $T - x$ plane. The tricritical point still appears but, as pointed out in Ref. [5], it is metastable.

Chapter 3

The Blume-Emery-Griffiths magnetic polymer model

3.1 BEG model on the SAW polymer

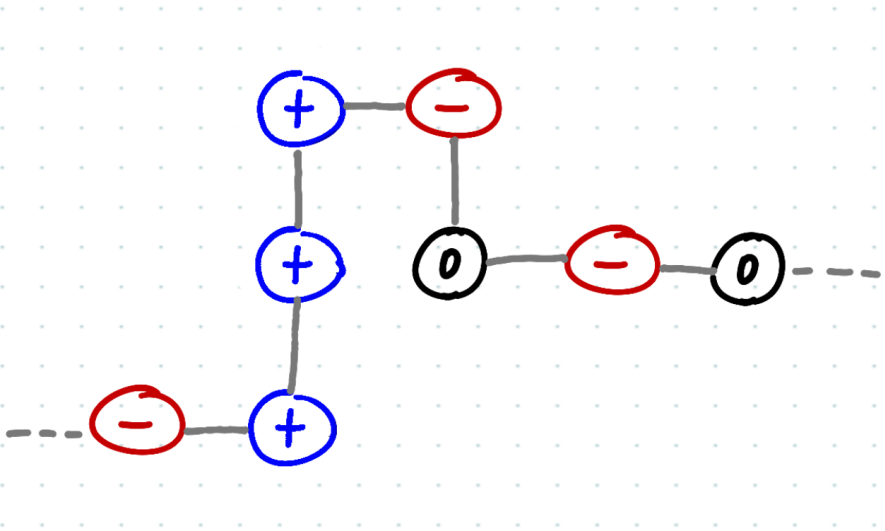

Figure 3.1: A sketch BEG magnetic polymer modeled as a self avoiding walk. Each monomer carry a spin variable $S_i \in \{0, \pm 1\}$ and their interaction is ruled by Eq. (3.2).

In this chapter we study a Blume-Emery-Griffith magnetic polymer model, i.e. we transpose the Blume-Emery-Griffith model from a lattice to the geometry of self avoiding walks. The Hamiltonian of the system is:

$$\mathcal{H}(\{S\}; J, K, \Delta) = -\frac{J}{2}\sum_{i,j} S_i \Lambda_{i,j} S_j - \frac{K}{2}\sum_{i,j} S_i^2 \Lambda_{i,j} S_j^2 + \Delta \sum_{i=1}^{N} S_i^2 - \Delta N \tag{3.1}$$

where $\Lambda_{i,j}$ is the adjacency matrix of the SAW, N is the length of the SAW and J, K and Δ are, as in the lattice BEG model, the ferromagnetic exchange energy, the strength of the biquadratic interaction and the chemical potential factor.
The approach will be the same of the previous chapter: firstly we will study in detail the two extremal limit $K/J \to 0$ and $K/J \to \infty$ and secondly we will show how the phase diagrams of the system change as a function of the ratio K/J. For each case we will draw the phase

diagram on the $T-\Delta$ and on the $T-x$ planes, paying attention to the different phases and to the appearance of critical, tricritical and triple points.
In the appendix, the mean field partition function and the mean field free energy density for the general case are derived in detail.

3.2 $K = 0$

In order to study a BEG magnetic polymer, we assign to each monomer a spin variable $S_i \in \{-1, 0, 1\}$. The Hamiltonian of such a system can be simply derived from the Hamiltonian of the standard BEG model (on the lattice) by simply adding to the ferromagnetic term the SAW adjacency matrix $\Lambda_{i,j}$ (Refs. [3, 4, 6, 7]):

$$\mathcal{H}_{K=0}(\{S\}; J, \Delta) = -\frac{J}{2}\sum_{i,j} S_i \Lambda_{i,j} S_j + \Delta \sum_{i=1}^{N} S_i^2 - \Delta N \tag{3.2}$$

where J is the ferromagnetic exchange energy, N is the length of the walk. The mean field partition function and the mean field free energy density are:

$$\mathcal{Z} \approx A \exp\left(N \log\frac{z}{e} - \frac{1-\rho}{\rho}\log(1-\rho) - \frac{\phi^2 N}{2\beta J z \rho} + N\log(1 + 2e^{-\beta\Delta}\cosh\phi) + \beta\Delta N \right) \tag{3.3}$$

$$f(\phi, \beta, \rho; J, \Delta) = -\frac{1}{\beta}\log\frac{z}{e} + \frac{1}{\beta}\frac{1-\rho}{\rho}\log(1-\rho) + \frac{\phi^2}{2\beta^2 J z \rho} - \frac{1}{\beta}\log\left(1 + 2e^{-\beta\Delta}\cosh\phi\right) - \Delta \tag{3.4}$$

It is interesting to notice that in the limit of no vacancies $\Delta \to -\infty$ one finds the same free energy density and the same self-consistent equation of the Ising magnetic polymer model (see Ref. [4]). From the previous definitions it is straightforward to derive the average magnetization per monomer m and the average concentration of vacancies x:

$$m = \langle S_i \rangle = \frac{2e^{-\beta\Delta}\sinh\phi}{1 + 2e^{-\beta\Delta}\cosh\phi} \tag{3.5}$$

$$x = 1 - \langle S_i^2 \rangle = -\frac{\partial}{\partial\Delta} f(\beta, \rho, \Delta) = \frac{1}{1 + 2e^{-\beta\Delta}\cosh(\phi)} \tag{3.6}$$

In the Appendix, we show some trivial results about the BEG polymer model when the polymer density ρ is fixed. The exact critical behavior of a lattice BEG model are recovered, with the unique difference that the critical temperatures are directly proportional to the polymer density ρ.
Let us minimize the free energy with respect to ϕ and ρ:

$$\frac{\partial f}{\partial \rho} = 0 \qquad \frac{\partial f}{\partial \phi} = 0 \tag{3.7}$$

This leads to the following mean field equations:

$$\log(1-\rho) = -\rho - \frac{\phi^2}{2\beta J z} \tag{3.8}$$

$$\phi = \beta J z \rho \frac{\sinh\phi}{\cosh\phi + \frac{e^{\beta\Delta}}{2}} \tag{3.9}$$

From Eq. (3.9) we can find a relation between the field ϕ and the average magnetization per monomer, giving a physical meaning to this field:

$$\phi = \beta J z \rho m. \tag{3.10}$$

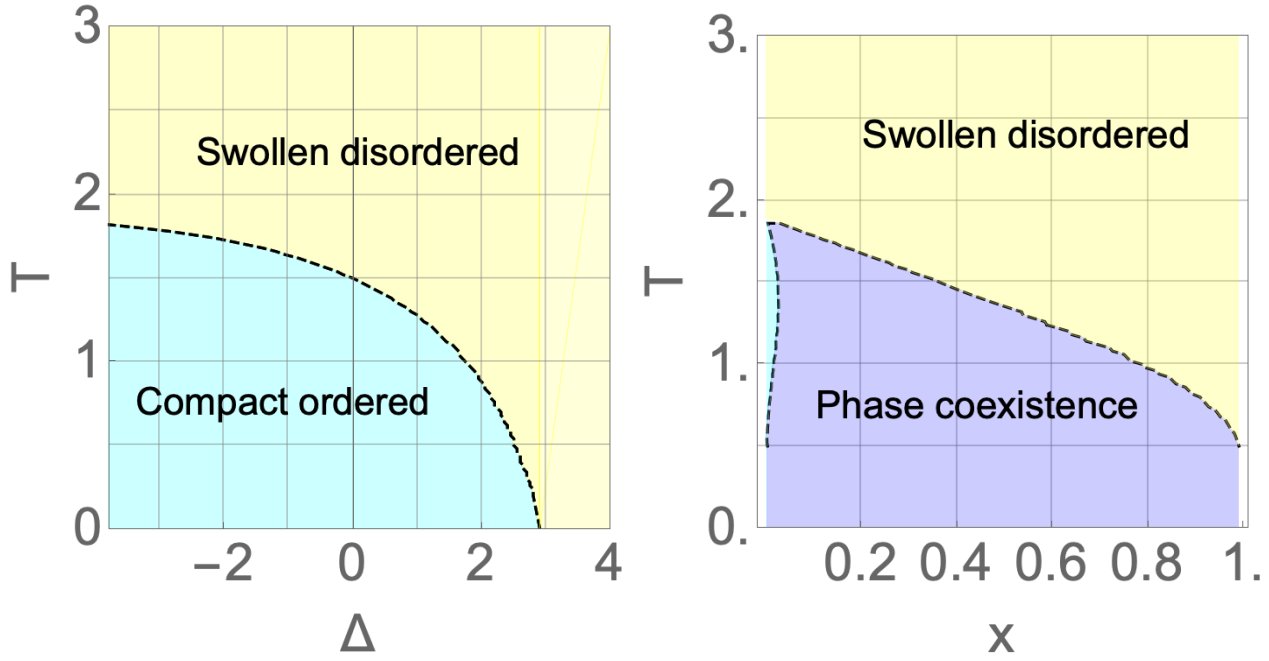

(a) (b)

Figure 3.2: In both panels, the ferromagnetic exchange energy has been set $J = 1$ and the coordination number to $z = 6$. (a): phase diagram of the BEG magnetic polymer when $K = 0$ on the T-Δ plane. A CO and a SD phase appear and they are separated by a discontinuous phase transition (black dashed line). (b): phase diagram on the T-x plane. Notice that the binodal lines extend also below $T = 0.5\,J$.

We are now interested in finding the solutions of the system of these two equations. Clearly $(\phi = 0, \rho = 0)$ is always a solution for each values of x and β. But there could be also other solutions with $\phi > 0$ and $\rho > 0$. In order to find them, numerical techniques have been exploited. The computed phase diagrams in the T-Δ and in the T-x planes are shown respectively in Figures 3.2(a) and 3.2(b). Only two phases appear: a compact ordered one (CO, where $\phi > 0$ and $\rho > 0$) and a swollen disordered one (SD, where $\phi \simeq 0$ and $\rho \simeq 0$) divided by a first order transition line. Notice that when $\Delta \to -\infty$, or equivalently, when $x \to 0$, the transition temperature approaches $T \approx 1.886J$: this result has been already obtained in Ref. [4] in the limit of a vanishing magnetic field h. It is interesting to look at the coefficients of the virial expansion of the free energy density:

$$B_2(\beta, \Delta) = \frac{1}{\beta} \tag{3.11}$$

$$B_3(\beta, \Delta) = \frac{1}{3\beta} - \frac{2z}{e^{\beta\Delta} + 2} \tag{3.12}$$

$$B_4(\beta, \Delta) = \frac{1}{4\beta} \tag{3.13}$$

$$\tag{3.14}$$

Whatever the values of the third and the fourth virial coefficients, the second one is always positive. Therefore no θ transitions are expected.

3.3 $J = 0$

In this limit the Hamiltonian reduces to:

$$\mathcal{H}_{J=0}(\{S\}; K, \Delta) = -\frac{K}{2}\sum_{i,j} S_i^2 \Lambda_{i,j} S_j^2 + \Delta \sum_{i=1}^{N} S_i^2 - \Delta N \tag{3.15}$$

Because of the absence of an ordering ferromagnetic term, we expect to observe only disordered phases. The mean field free energy density is:

$$f(\alpha, \beta, \rho; K, \Delta) = -\frac{1}{\beta}\log\frac{z}{e} + \frac{1}{\beta}\frac{1-\rho}{\rho}\log(1-\rho) + \frac{\alpha^2}{2\beta^2 z K \rho} - \frac{1}{\beta}\log(1 + 2e^{-\beta\Delta+\alpha}) - \Delta \tag{3.16}$$

The average concentration of vacancies is given by:

$$x = \frac{1}{1 + 2e^{-\beta\Delta+\alpha}}. \tag{3.17}$$

Minimizing Eq. (3.16) with respect to α and ρ:

$$\frac{\partial f}{\partial \alpha} = 0 \qquad \frac{\partial f}{\partial \rho} = 0 \tag{3.18}$$

we find the following mean field equations:

$$\frac{\alpha}{\beta K z \rho} - \frac{1}{\frac{e^{\beta\Delta-\alpha}}{2} + 1} = 0 \tag{3.19}$$

$$\rho + \log(1-\rho) + \frac{\alpha^2}{2\beta z K} = 0 \tag{3.20}$$

From Eqs. 3.17 and 3.19 we can derive a relation among the field α and the average concentration of vacancies:

$$\alpha = \beta K z \rho (1 - x). \tag{3.21}$$

By Taylor expanding the $\log(1-\rho)$ terms around $\rho = 0$ up to the second order we can derive an approximated relation between the field α and the polymer density ρ:

$$\alpha \approx \sqrt{\beta K z}\rho. \tag{3.22}$$

Plugging in Eq. (3.16) and expanding around $\rho \approx 0$ we can easily derive the virial expansion, whose second and third virial coefficients are:

$$B_2(\beta, \Delta) = \frac{1}{\beta} - \frac{2\sqrt{\beta K z}}{\beta\left(e^{\beta\Delta} + 2\right)} \tag{3.23}$$

$$B_3(\beta, \Delta) = \frac{1}{6\beta} - \frac{K z e^{\beta\Delta}}{\left(e^{\beta\Delta} + 2\right)^2} \tag{3.24}$$

$$B_4(\beta, \Delta) = \frac{1}{12\beta} - \frac{K z e^{\beta\Delta}\left(e^{\beta\Delta} - 2\right)\sqrt{\beta K z}}{3\left(e^{\beta\Delta} + 2\right)^3} \tag{3.25}$$

$$\tag{3.26}$$

The point at which both the second and the third virial coefficient vanish (the fourth virial coefficient is instead positive) is:

$$(T^*, \Delta^*) = (\frac{9}{16}Kz, -\frac{9}{16}Kz\log\frac{3}{2})$$

Moreover, we expect a continuous transition in density when $B_2(T,\Delta) = 0$ and $B_3(T,\Delta) > 0$. Defining $x(\alpha = 0)$ as the concentration of vacancies in the $\alpha = 0$ phase (no interactions, it is expected to be the swollen phase):

$$x(\alpha = 0) = \frac{1}{1 + 2e^{-\beta\Delta}} \tag{3.27}$$

one can easily recover the previous conditions on the T-x plane. The point at which the two virial coefficients vanish is:

$$(T^*, x^*) = (\frac{9}{16}Kz, \frac{1}{4})$$

and moreover the critical line is:

$$T = zK(x-1)^2 \qquad x < \frac{1}{4} \tag{3.28}$$

In Figures 3.3(a) and 3.3(b) we show the numerically computed mean field phase diagrams. There is a continuous transition between a compact (disordered) phase and a swollen (disordered) phase which becomes discontinuous if the concentration of vacancies is higher than a critical value (in this case, 1/4). Moreover the slope of the transition line is continuous at the tricritical point (as in the standard lattice BEG model).

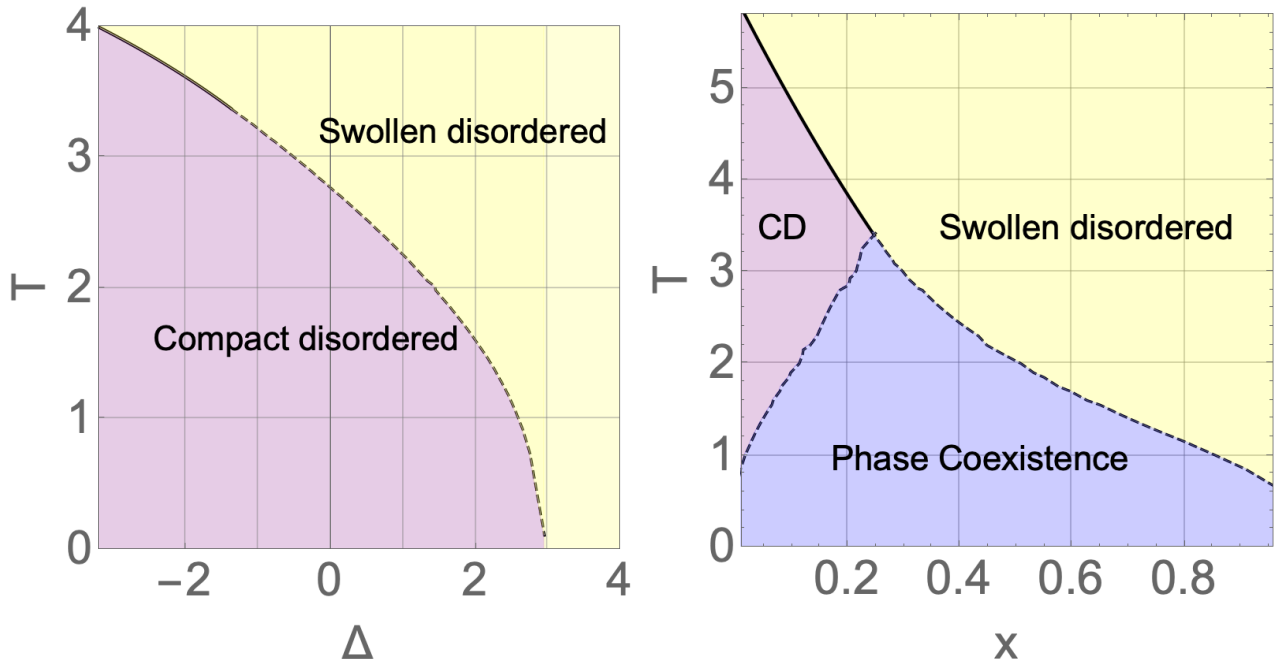

(a) (b)

Figure 3.3: For these plots $K = 1$ and $z = 6$. (a): phase diagram on the $T - \Delta$ plane. The separation line between the two phases is split by a multicritical point. (b): phase diagram on the $T - x$ plane.

3.4 Intermediate cases

In this section we consider the full BEG model on the polymer with both the ferromagnetic and the biquadratic interaction terms in the Hamiltonian.

The mean field free energy per monomer is:

$$f(\phi,\alpha,\beta,\rho;J,K,\Delta) = -\frac{1}{\beta}\log\frac{z}{e} + \frac{1}{\beta}\frac{1-\rho}{\rho}\log(1-\rho) + \frac{1}{2\beta^2 z\rho}\left(\frac{\phi^2}{J}+\frac{\alpha^2}{K}\right) - \frac{1}{\beta}\log(1+2e^{-\beta\Delta+\alpha}\cosh(\phi)) - \Delta. \quad (3.29)$$

As in the previous cases, the magnetization per spin m and the average concentration of vacancies x are given by:

$$m = \frac{2e^{-\beta\Delta+\alpha}\sinh\phi}{1+2e^{-\beta\Delta+\alpha}\cosh\phi} \quad (3.30)$$

$$x = \frac{1}{1+2e^{-\beta\Delta+\alpha}\cosh\phi} \quad (3.31)$$

The mean field phase diagrams can be studied by numerically solving the following mean field equations:

$$\frac{\partial f}{\partial\phi}=0 \qquad \frac{\partial f}{\partial\alpha}=0 \qquad \frac{\partial f}{\partial\rho}=0 \quad (3.32)$$

$$\frac{\phi}{\beta Jz\rho} - \frac{\sinh(\phi)}{\frac{e^{\beta\Delta-\alpha}}{2}+\cosh(\phi)} = 0 \quad (3.33)$$

$$\frac{\alpha}{\beta Kz\rho} - \frac{\cosh(\phi)}{\frac{e^{\beta\Delta-\alpha}}{2}+\cosh(\phi)} = 0 \quad (3.34)$$

$$\rho + \log(1-\rho) + \frac{1}{2\beta z}\left(\frac{\phi^2}{J}+\frac{\alpha^2}{K}\right) = 0 \quad (3.35)$$

In order to reach a detailed knowledge of the different kind of phase diagrams that appears it is worth to use again the virial expansion. For the CD - SD transition we have already seen what happens in the case $K/J \to \infty$. Here we focus on the transition between the CO and the CD phase. Dividing Eq. (3.34) by Eq. (3.33) we can derive a relation between the field α and the field ϕ:

$$\alpha(\phi) = K/J\phi\coth\phi$$

Plugging this relation in Eq. (3.33) and Taylor expanding around $\phi \approx 0$ up to the third order it is possible to write the field $\phi = \phi(\rho)$ in terms of the polymer density ρ. It is thus possible to Taylor expand the free energy density around the value of polymer density ρ^* such as $\phi(\rho^*) = 0$. In this case:

$$\rho^* = \frac{(2e^{-\beta\Delta+K})+1}{2ze^{-\beta\Delta+K}}T$$

Unfortunately it is not possible to derive an explicit analytical formula of the virial coefficients because of the computational complexity. However it is possible to derive the values of the coefficient numerically in each point of the phase diagram, by simply selecting a temperature T and a value of Δ.
As seen previously, we expect a continuous transition when the second virial coefficient vanishes and the third is positive. In Figure 3.4 it is possible to observe different situations: the red and the blue lines represent respectively the points of the T-Δ plane where the second and the third virial coefficient vanish. Below the blue curve the third virial coefficient is negative (all the considerations have been made selecting $z = 6$).

- When $K/J \simeq 0$, the second coefficient vanishes when the third is negative; therefore we do not expect any continuous transition between the ordered and the disordered compact phases;

- When $K/J \approx 1.8$ the two curves intersects in one point for low values of Δ;
- When $K/J \approx 2.88$ we expect a line of critical θ points when the red line lies above the blue one. A multicritical point occurs at the intersection of the two curves;
- Increasing again the ratio, the red line will be completely above the blue one and only a continuous transition is expected between the disordered and the ordered phase.

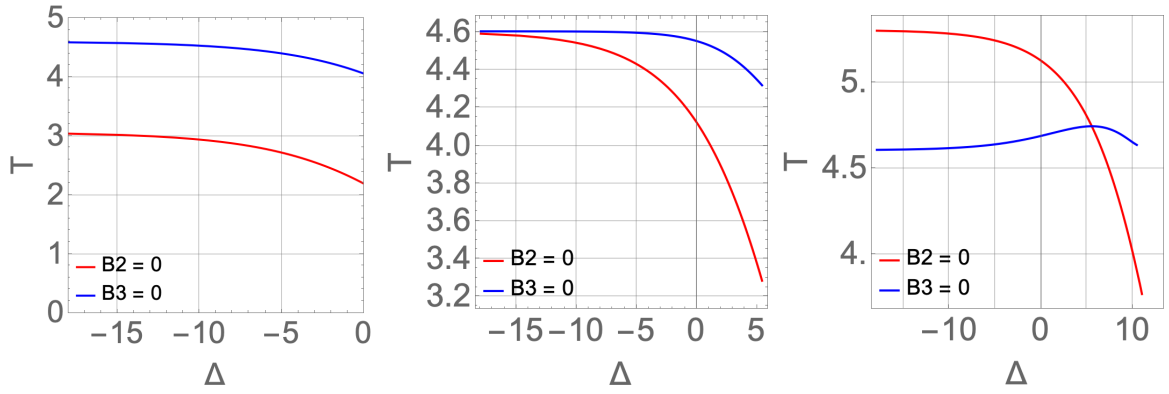

Figure 3.4: In all these graphs, $J = 1$ and $z = 6$. Lines represent the points where the second and third virial coefficients vanish (respectively red and blue), for different values of the ratio K/J. The third virial coefficient is negative below the blue line. (a): $K/J = 0.8$. The red line lies below the blue line: no θ transitions are expected; (b): $K/J = 1.8$: the two curves are near to each other. Therefore (at least, in the range of Δ selected for this picture, no continuous transitions between the compact phases are expected; (c): $K/J = 2.88$: a multicritical point occurs when the two curves intersect each other.

$K/J = 0.8$

When the ratio increases again, the properties of the $J = 0$ limit start to appear. In fact, a compact disordered CD phase starts to appear. For instance see Figure 3.5: the transition between the CO and the CD phase is still discontinuous because of the negativity of the third virial coefficient (see first panel in Figure 3.4). Moreover, the transition between the CD and the SD phase is continuous, in fact the tricritical point of the $K/J \to \infty$ limit case is expected to be at an $x = 1/4$.

$K/J = 1.8$

For $K/J = 1.8$ the peculiarities of both the two limiting cases appear in the same phase diagram; see for instance Figure 3.6. In particular, the red line of Figure 3.4 is still below the blue one in the range of Δ considered in Figure 3.6 therefore we see a discontinuous transition between the CO and the CD phase. Moreover, the transition line between the CO and the CD phase extends in the region $x > 1/4$ where it is actually discontinuous. This means that there are two interesting points in the phase diagram:

- a triple point, where a CO phase coexists together with a CD and a SD phase. From Figure 3.6 the coordinates of such a point are $(\Delta \approx 1.95, T \approx 3.95)$. In the panel b of the figure, the isochemical line $\Delta = 1.95$ has been drawn inside the phase coexistence region;
- a tricritical point in the line between the CD and the SD phases.

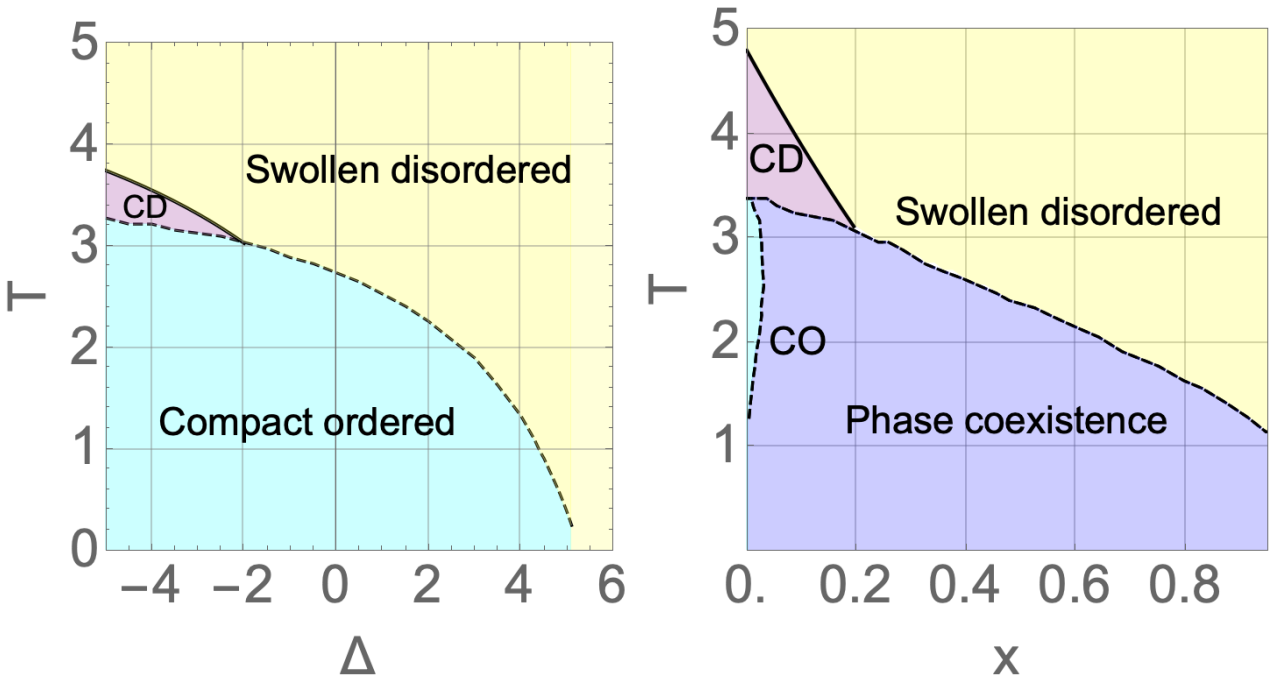

(a) (b)

Figure 3.5: In these graphs $J = 1$ and $z = 6$. (a): $T - \Delta$ phase diagram with $K/J = 0.8$. Notice the appearance of the CD phase. (b): $T - x$ phase diagram with $K/J = 0.8$.

Moreover, in Figure 3.7, the free energy landscape for $\Delta = 1.95$ and different values of the temperature T have been plotted. When $T = 3.95$ it is possible to appreciate three minimum at the same height of the free energy, for three different values of ρ: the two values $\rho > 0$ correspond to the CD (the lower) and the CO (the greater) phase; the $\rho \approx 0$ minimum correspond to the SD phase.

$K/J = 2.88$

Increasing again the ratio, a continuous line starts to appear between the CO and the CD phase (see Figure 3.8(a)). The triple point is no more present in the phase diagram, in fact there are no points where three first order transition lines intersect; the tricritical point of the limit $K/J \to \infty$ still appears (see Figure 3.8(b)).

3.5 Discussion

This phenomenology is very rich, as in the original lattice BEG model. Why these results are interesting? There are at least three reasons:

- A compact disordered (CD) phase was obtained, within the Ising/Potts magnetic polymer model, only when the system was driven out-of-equilibrium (see Ref. [3]) or adding an overall positive contribution to the Hamiltonian (the parameter c in Ref. [6]). Here instead such a phase is observed in equilibrium, for certain values of the strength of the biquadratic interaction;
- A tricritical point in the transition line between a CD and a SD phase is observed. In the papers cited before, such a transition was genuinely continuous;

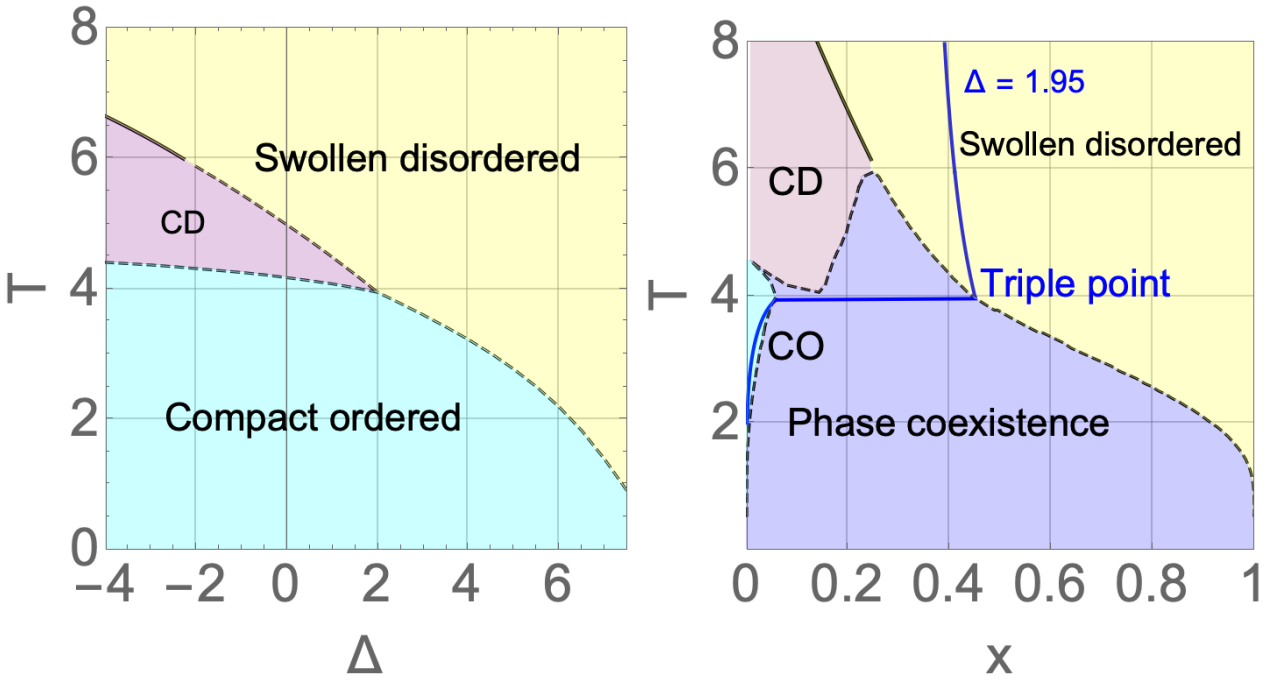

(a) (b)

Figure 3.6: In these graphs, $J = 1$ and $z = 6$. (a): $T - \Delta$ phase diagram with $K/J = 1.8$. Both a tricritical point and a triple point appear in the same phase diagram. The first one lies on the separation line between the CD and the SD phase; the second point is at the conjunction of the three dashed lines. (b): $T - x$ phase diagram. A isochemical line $\Delta = 1.95$ has been drawn to stress the presence of a triple point in the phase diagram.

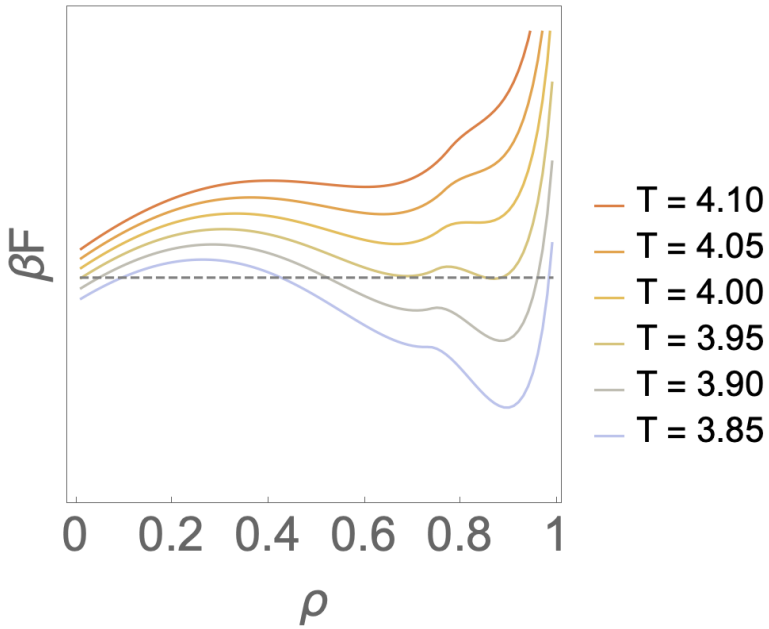

Figure 3.7: Free energy landscapes of the mean field free energy density related to the ratio $K/J = 1.8$ as a function of the polymer density. The value of $\Delta = 1.95$ is the same for every curve. The triple point condition can be observed on the $T = 3.95$ landscape where the three minima of the free energy density have the same height. The two minima at $\rho > 0$ correspond to the compact phases; the other one at $\rho = 0$ corresponds to a swollen disordered phase.

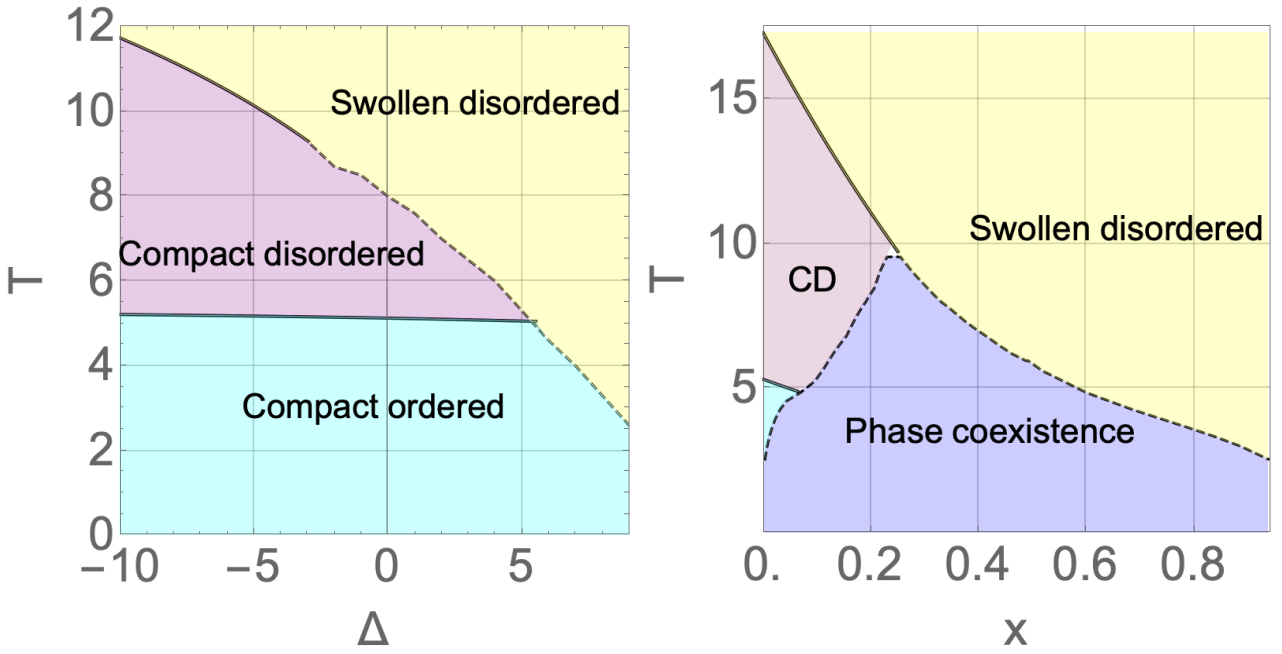

(a) (b)

Figure 3.8: For these plots, $J = 1$ and $z = 6$. (a): mean field phase diagram of the BEG magnetic polymer when $K/J = 2.88$ on the T-Δ plane. A tricritical point appears on the CD - SD transition line. Notice that in this situation the triple point does not appear anymore. (b): mean field phase diagram on the T-x plane.

- A triple point between all the three phases is predicted in the mean field phase diagram when $K/J \approx 1.8$.

How we can transpose these results in the field of the biophysics of the chromatin? Chromatin is a giant polymer located in the cellular nucleus (see Ref. [8]). Its monomers are the nucleosomes, made of a DNA filament twisted around a protein called histone. When an histonic marker (named also epigenetic markers) attaches to an histone, it induces a local modification of the chromatin. Historically, two types of chromatin have been identified: eterochromatin, extremely dense and compact, and euchromatin, less packed. Both these two types are characterized by specific historic markers, inducing for instance, a local folding in the former and a local expansion in the latter.
The polymeric substrate of our magnetic polymer model can be thought as a representation of the chromatin molecule, with each monomer corresponding to a nucleosome. Following Ref. [6] we can associate to a state with $S_i = 0$ a non-modified histone and to a state with $S_i = \pm 1$ an histone modified by one of the two most relevant eterochromatin histone markers (H3K9me3 and H3K27me3). The presence of a CO phase could be related to an highly packed chromosome, whose histones are decored with almost one of the two heterochromatin histone markers, where the biological processes of the transcription and translation cannot occur; a swollen disordered phase could represent an open chromosome, not decored at all with markers and ready to be transcribed; a compact disordered phase could be thought as an intermediate semi - compact phase (remember that in the CD phase the polymer density ρ is typically lower than in the CO phase) decorated with both the types of eterochromatin histone markers. Region of phase coexistence between compact and swollen phases could be interpreted as a chromosome with some regions highly packed and others much more open.

Chapter 4

Monte Carlo simulations

In this chapter, we show the results of our Monte Carlo simulations of the Blume-Emery-Griffith magnetic polymer. In the first section the principles of such simulations are described; in the following sections these results are compared with the mean field predictions of the previous chapter.

4.1 Principles

As seen in the previous chapters, the physics of magnetic polymers is determined by the interplay between magnetic and conformational degrees of freedom. Therefore, our Monte Carlo method takes into account both:

- the evolution of the magnetic states;
- the changes of the polymeric substrate, i.e. of the SAWs representing the polymer.

The first part of the method is simply implemented as a standard Metropolis algorithm. In particular, a Metropolis move consists in selecting a monomer, change the value of its spin variable and accepting the new configuration according to the energy variation ΔE: the move is in fact accepted with probability $\min(1, \exp(-\beta\Delta E))$.
Regarding the second part, in our simulations we will consider SAWs on a three-dimensional cubic lattice (the coordination number is $z = 6$). We start our simulation from a linear walk and, by using an appropriate Markovian process, we evolve this chain until it has reached the equilibrium distribution. In order to do this, we use a combination of local and non local moves:

- *Local moves*: alter the configuration of a few consecutive monomers at the same time, leaving the other vertices unchanged. We consider one bead flips, known also as *corner moves*, and two beads *crankshafts moves* (see Figure 4.1(a) for examples). A local move is accepted with probability $\min(1, \exp(-\beta\Delta E))$ where ΔE is the energy difference.
- *Pivots*: change the configuration of a great number of beads at the same time. We choose randomly a monomer along the chain as a pivot point, and apply randomly one of the possible symmetries of the cubic lattice (e.g. rotations and reflections), on all the sites following our pivot point (see Figure 4.1(b)). Such kind of moves are necessary to ensure the ergodicity of the system. As before, the new configuration is accepted with probability $\min(1, \exp(-\beta\Delta E))$ (see Ref. [9] for details).

Let us expose in detail our algorithm. For each case we have studied, we have performed simulations for the following polymer sizes: $N = 50, 100, 200, 300, 400$. We start from an initial

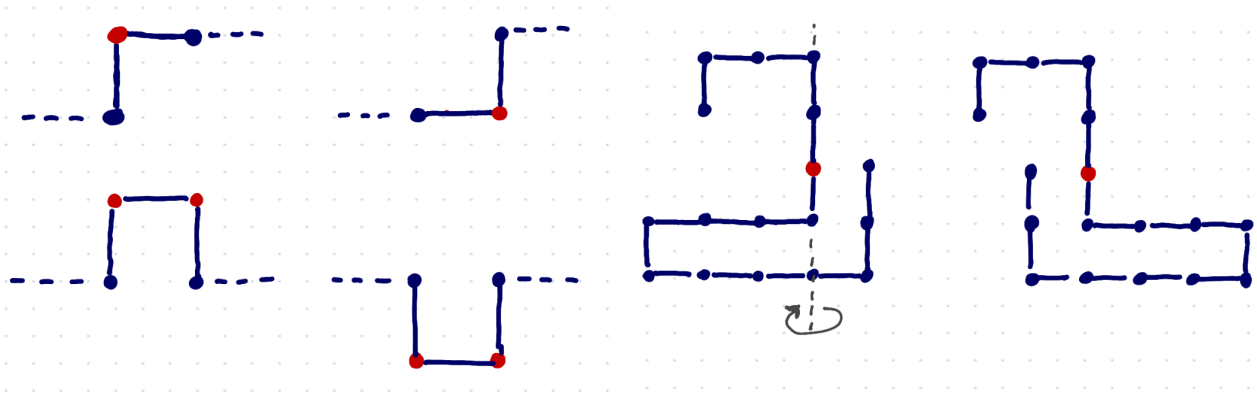

(a) (b)

Figure 4.1: Examples of two dimensional moves for the Monte Carlo simulations. (a): Local moves: above is shown a corner moves where the position of just one bead is changed; below it is shown a crankshafts move, where two beads are moved. (b): A pivot move: the pivot is the red bead. All the beads below it are subjected to a reflection with respect to the vertical axes.

straight linear magnetic polymer, whose spin variables are random. A Monte Carlo sweep consists of the following passages:

1. A pivot is attempted;
2. We attempt N local moves;
3. We span all the monomers of the polymer and attempt a Metropolis move for each of them.

In order to relax the system, in Ref. [10] it is suggested to perform at least $10^2 \cdot N$ Monte Carlo steps. In our simulations, we have set the number of relaxation Monte Carlo steps to 10^5 for each N. We choose the total length of the simulations t to be at least 500 times the maximum autocorrelation times of the observables computed during the execution.
To speed-up the convergence of the algorithm we employ the Multiple Markov Chain strategy i.e. we run in parallel M Markov Chains at different temperatures T_i with $i = 1, 2, \ldots, M$. After each Monte Carlo sweep, we attempt to exchange configurations between adjacent pairs of chains T_i, T_{i+1} with probability:

$$p = \min(1, \exp((\beta_{i+1} - \beta_i)(E_{i+1} - E_i)). \tag{4.1}$$

The main advantage of this kind of strategy is that it leads to an algorithm where metastable states can be overcome, as the chains in these states can be swapped away at other higher temperatures. Thanks to this fact, the equilibration time and the autocorrelation time are sensibly reduced with respect to the single chain procedure. In our simulations we run in parallel $M = 30$ different chains.
The interesting observables computed during the simulations are the following:

- *Specific heat at fixed volume* c_V. Given $\langle E_T \rangle$ the average energy at temperature T, the specific heat is defined as:

$$c_V = \frac{1}{N} \frac{\partial E_T}{\partial T} = \frac{\langle E^2 \rangle_T - \langle E \rangle_T^2}{N k_B T^2} \tag{4.2}$$

- *Average number of contacts* n_c *and variance* C:

$$C = \frac{\langle n_c^2 \rangle - \langle n_c \rangle^2}{N} \tag{4.3}$$

Cleary, if the number of contacts is small, the polymer will be in a swollen, open phase. On the other hand, a compact polymer will display a large number of contacts. Peaks in the graph of C vs T give us information about the swollen - ordered transition temperature.

- *Average magnetization per monomer* m *and magnetic susceptibility* χ_M defined as:

$$\chi_M = \frac{\langle m^2 \rangle - \langle m \rangle^2}{k_B T}. \tag{4.4}$$

Peaks on the graph χ_M-T give us information on the ordered - disordered transition temperature.

- *Average concentration of vacancies* x, defined as:

$$x = 1 - \frac{1}{N} \sum_{i=1}^{N} S_i^2 \tag{4.5}$$

where $S_i \in \{0, \pm 1\}$ is the spin variable carried by the i-th monomer.

- *Average radius of gyration* $\langle R_G \rangle$: let $\mathbf{R}_i$ be the position of the i-th monomer. The center of mass of an homogeneous polymer $\mathbf{R}_{CM}$ is:

$$\mathbf{R}_{CM} = \frac{1}{N} \sum_{i=1}^{N} \mathbf{R}_i. \tag{4.6}$$

The radius of gyration is defined as:

$$R_G^2 = \frac{1}{N} \sum_{i=1}^{N} \|\mathbf{R}_i - \mathbf{R}_{CM}\|^2 \tag{4.7}$$

and it is subjected to important scaling laws: in a good solvent $R_G \propto N^{0.6}$ (the polymer is swollen), at the θ point $R_G \propto N^{0.5}$ and in a bad solvent $R_G \propto N^{1/3}$ (the polymer is compact, resembling a sphere). Thus looking at the properties of these scaling we can get information about the compact - swollen transition.

4.2 Results

4.2.1 $K/J = 0$

From the mean field phase diagram Figure 3.2(a), we expect a discontinuous phase transition for $\Delta < 3$ between a CO and a SD phase. Let us apply our protocol to $\Delta = 0$ and $\Delta = 1$. When $\Delta = 0$ the mean field transition temperature is $T \approx 1.5\, J$. In Figure 4.2(a) we show the specific heat in the range $0.8J < T < 2J$. Increasing the size N of the system, the peak becomes sharper and it tends to the mean field value of the transition temperature. We observe the same behavior in the graph of the magnetic susceptibility (in Figure 4.2(b)). It can be shown (see Ref. [4]) that the shift ΔT of the transition temperature from its value at $N = \infty$ goes like $\Delta T \sim 1/N$. In Figure 4.2(c) the temperature corresponding to the maximum of the magnetic susceptibility for all the values of N has been plot in function of $1/N$. From a linear interpolation it is possible to infer the value of the transition temperature looking at the intersection between the linear fit and the $1/N = 0$ vertical line. In order to avoid finite size effects, we have considered the first three points, corresponding to $N = 200, 300$ and 400. The estimation of the transition temperature is $T \approx 1.53\, J$, very similar to the mean field transition

temperature.
Given the value of R_g^2 for different values of the temperature, it is possible to verify the scaling laws written above. In Figures 4.3(a) and 4.3(b) we show that the graphs of $R_g^2/N^{2/3}$ computed for different size of the polymer collapse on each others for low temperatures. The same occurs at high temperatures to the graphs of $R_g^2/N^{1.2}$. It is also possible to exploit the intersections of the curves of R_g^2/N for different size of the systems to get an estimation of the transition temperature from configurational properties of the system (see Figure 4.3(c)). In Figure 4.4 we show the trend of the magnetization per spin m and of the concentration of vacancies x for $N = 200$. The transition occur again around $T = 1.5\,J$. In the plot are represented also a snapshot of a compact ordered configuration of our BEG polymer (in the bottom left corner) and a swollen disordered configuration (below the plot key): blue is associated to a spin variable $S_i = +1$, gray to $S_i = 0$ and red to $S_i = -1$.

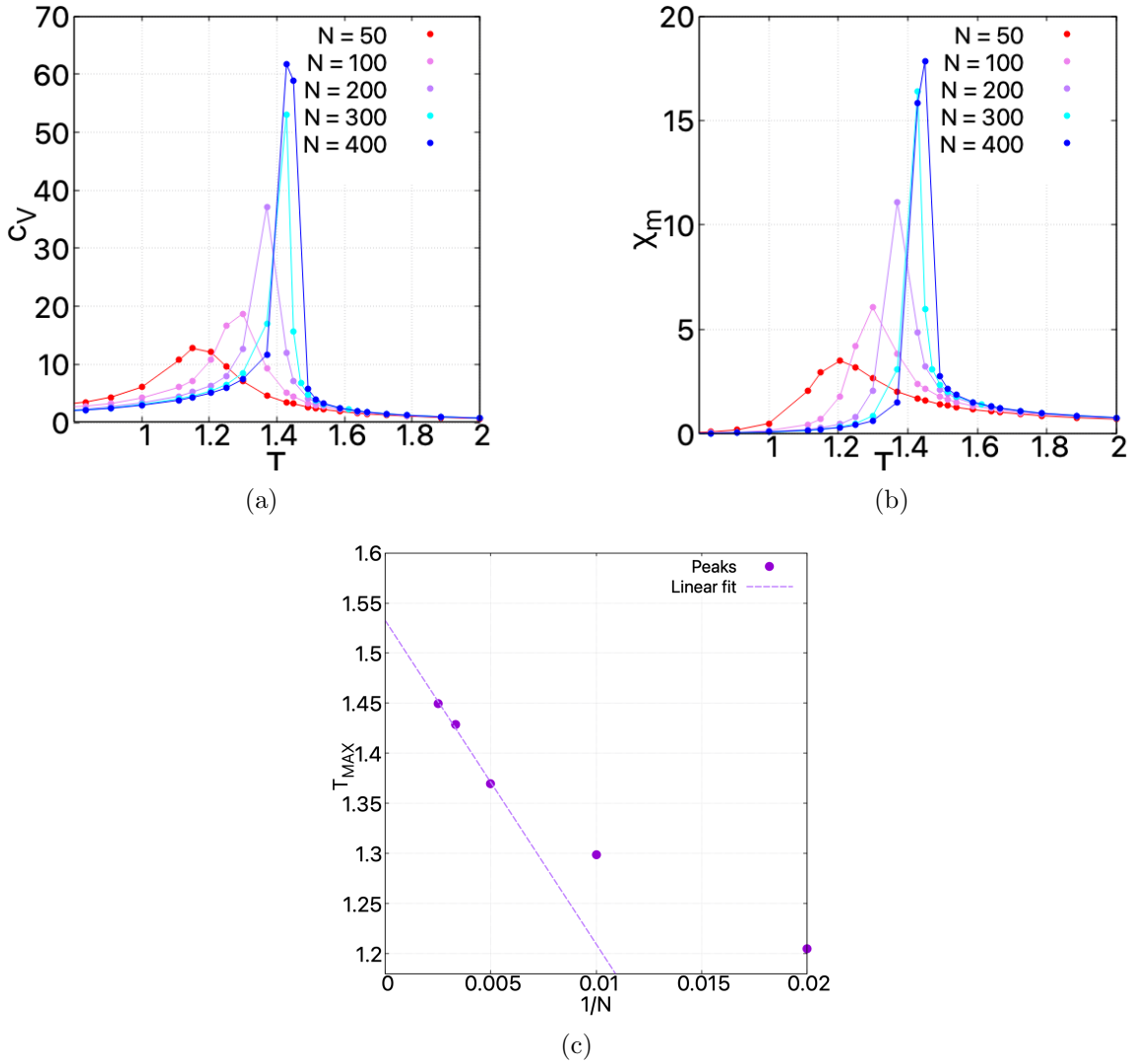

Figure 4.2: $K/J = 0$ and $\Delta = 0$. (a): Specific heat vs temperature. Increasing the size of the system the maximum of the specific heat tends to the mean field value of the transition temperature, i.e. $T \approx 1.5$. (b): Magnetic susceptibility vs temperature. Also in this case increasing the size of the system the maximum of χ_M tends to the mean field value. (c): Temperature of the maximum of the magnetic susceptibility vs $1/N$. A linear fit, taking into account only the first three points ($N = 200, 300$ and 400) in order to avoid finite size effects, is represented with a purple dashed line. The estimated transition temperature is $T \approx 1.53\,J$.

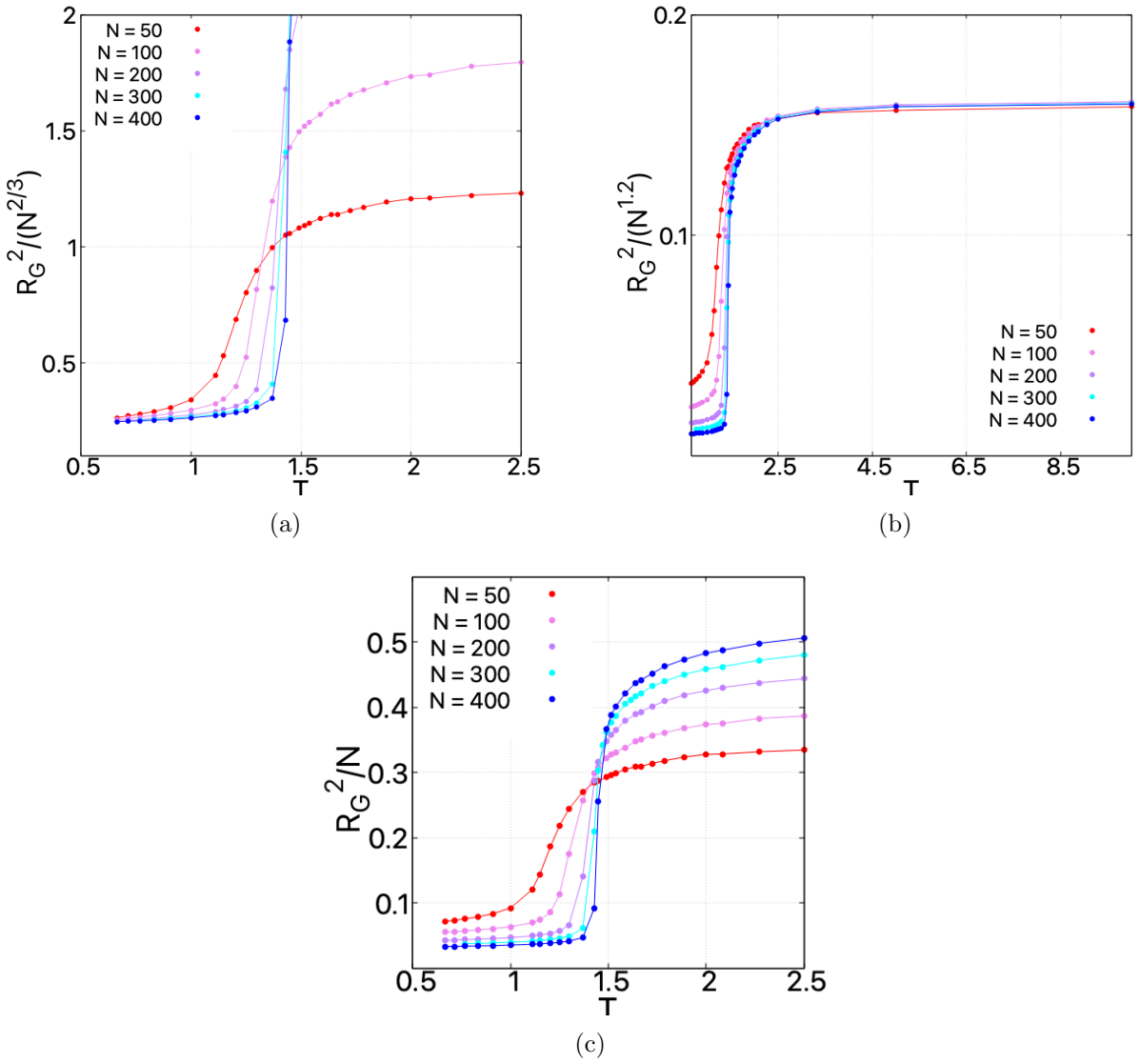

Figure 4.3: $K/J = 0$ and $\Delta = 0$. (a): Squared radius of gyration divided by $N^{2/3}$ vs temperature T. Notice how, for low temperatures, the curves collapse on each other. (b): Squared radius of gyration divided by $N^{1.2}$ vs temperature T. We observe a collapse at high temperature. (c): Squared radius of gyration divided by N vs temperature T.

For $\Delta = 1$ we expect a transition temperature of $T \approx 1.2J$. Both the specific heat and the magnetic susceptibility, computed with a size $N = 400$, show a peak at such a temperature (see Figure 4.5(a)). A transition is observable also in the trend of the average magnetization per spin m and of the average concentration of vacancies x (see Figure 4.5(b)).

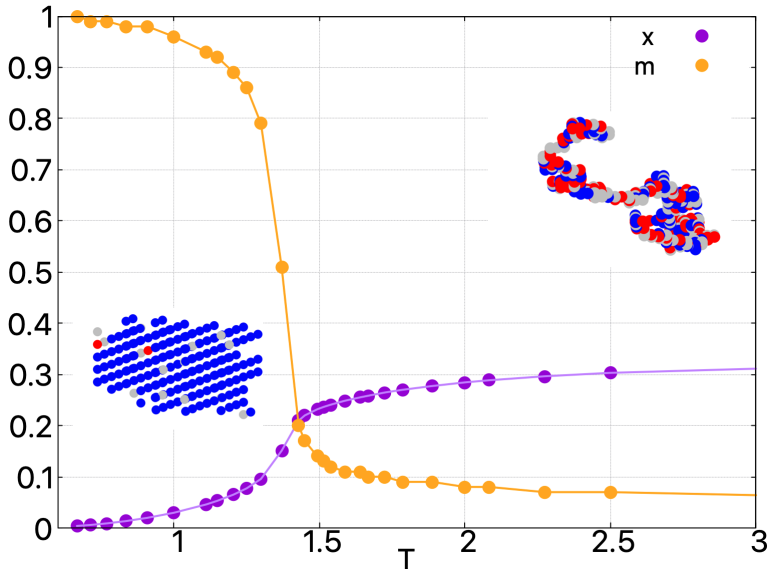

Figure 4.4: $K/J = 0$ and $\Delta = 0$. Average magnetization per spin and average concentration of vacancies with respect to the temperature for $N = 200$. Two configurations of the polymer are shown inside the plot: blue beads carry a +1 spin variable, gray ones carry a 0 spin variable and red ones a -1 spin variable. On the left we show a compact ordered phase; on the right a swollen disordered is represented.

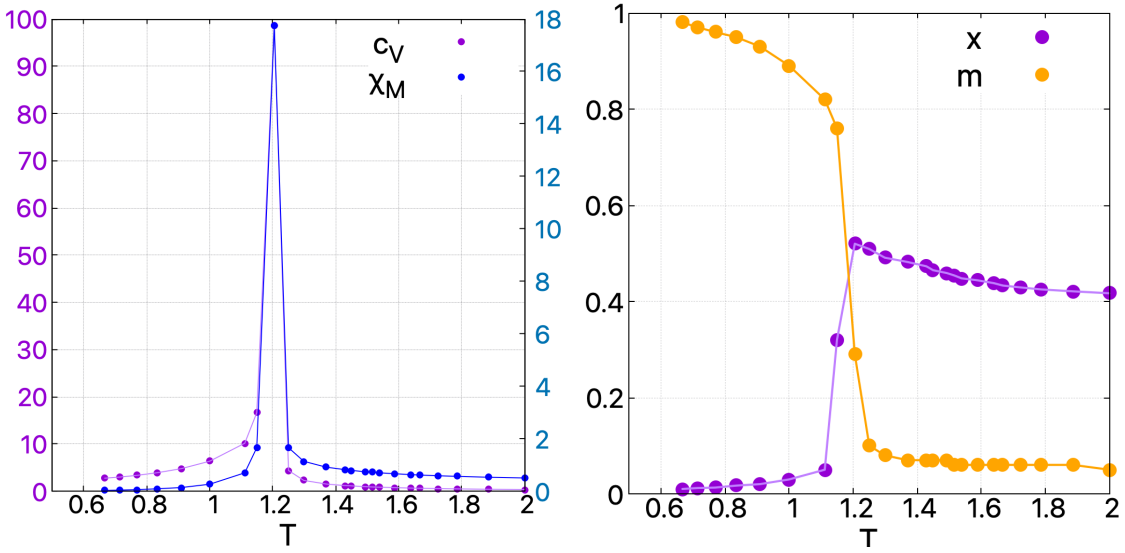

(a) (b)

Figure 4.5: $K/J = 0$ and $\Delta = 1$ and $N = 400$. (a): Specific heat (purple) and magnetic susceptibility (blue) as a function of temperature. (b): Average magnetization per spin and average concentration of vacancies as a function of temperature.

4.2.2 $K/J = 2$ and $\Delta = 0$

The mean field phase diagram of the BEG magnetic polymer when $K/J = 2$ is of the same kind of Figure 3.6(a). When $\Delta = 0$ we should observe two first order phase transitions: a CO - CD transition at a temperature $T \approx 4.5\,J$ and a CD - SD transition at $T \approx 5.5\,J$.
In Figure 4.7 we show the specific heat c_V of our system computed in the range $1.5\,J < T < 7\,J$ for different sizes N of the system. By increasing N the presence of the second transition is more evident.
By computing the magnetic susceptibility and the variance of the contacts it is possible to observe individually the ordered - disordered and the compact - swollen transition respectively. In Figure 4.8 one can appreciate that the peak in the magnetic susceptibility χ_M is located at the same temperature of the first peak in graph of the specific heat Figure 4.7; similarly the peak in Figure 4.9 corresponds to the second peak in Figure 4.7.
Unfortunately, the temperatures at which both the transitions occur in the Monte Carlo simulation are lower with respect to the predictions coming from the mean field phase diagram (see for instance the scaling analysis in Figure 4.6, where the estimated transition temperatures are $T_1 \approx 3.4\,J$ for the CO-CD transition and $T_2 \approx 4.5\,J$ for the CD-SD one). However we remark that those phase diagrams have been computed within the maen field approximation.

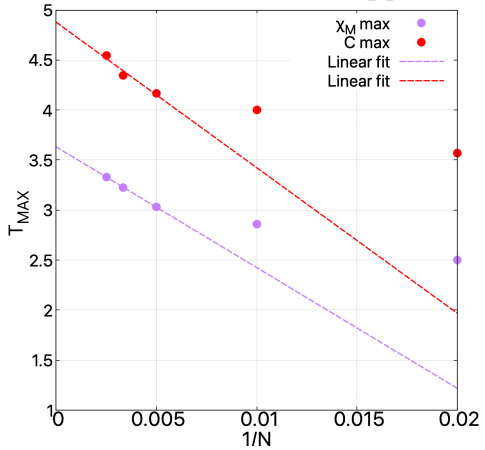

Figure 4.6: $K/J = 2$ and $\Delta = 0$. Temperatures of the maximum of the magnetic susceptibility and of the variance of contacts vs $1/N$. Linear fits are represented with dashed lines.

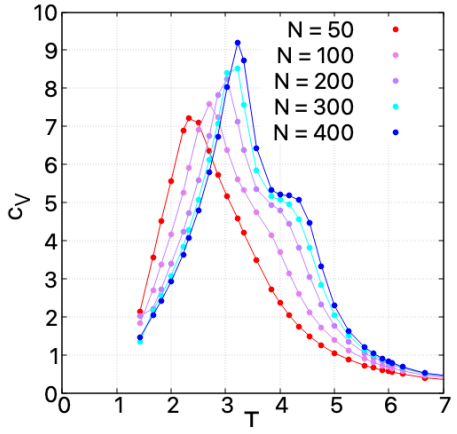

Figure 4.7: $K/J = 2$ and $\Delta = 0$. Specific heat vs temperature.

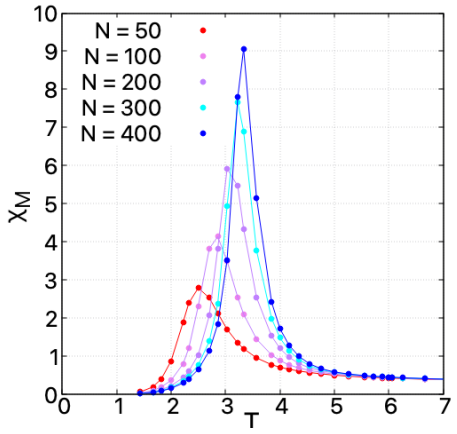

Figure 4.8: $K/J = 2$ and $\Delta = 0$. Magnetic susceptibility for different values of the temperature.

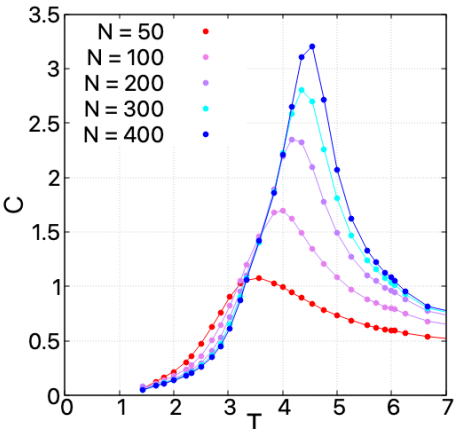

Figure 4.9: $K/J = 2$ and $\Delta = 0$. Variance of the number of contacts for different values of the temperature.

4.2.3 $K/J = 3$ and $\Delta = 0$

The mean field phase diagram of the BEG magnetic polymer when $K/J = 3$ is of the same kind of Figure 3.8(a). In this case, when $\Delta = 0$ we should observe a CO - CD transition at a temperature $T \approx 5.5\,J$ and a CD - SD transition at $T \approx 8.0\,J$.
In Figure 4.10 the trends of the average magnetization per spin and of the average concentration of vacancies are shown for $N = 400$, both characterizing the first of the two transitions (CO-CD). The transition seems to occur at a temperature around $T_1 \approx 4.0\,J$. More details can be obtained from Figure 4.11, where we show the specific heat c_V of our system computed in the range $1J < T < 10J$ for different sizes N of the system. By increasing N the two peaks (and also the minimum between them) become sharper and sharper. Notice in particular that the first peak is higher than the second one: this is coherent with the fact that the CO - CD phase transition is expected to be continuous.
In Figure 4.12 one can appreciate that the peak in the magnetic susceptibility χ_M is located at the same temperature of the first peak in graph of the specific heat Figure 4.11; similarly the peak in Figure 4.13 corresponds to the second peak in Figure 4.11.

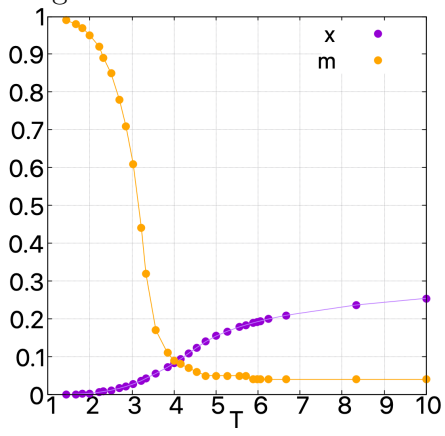

Figure 4.10: $K/J = 3$ and $\Delta = 0$. Average magnetization per spin and average concentration of vacancies with respect to the temperature for $N = 400$.

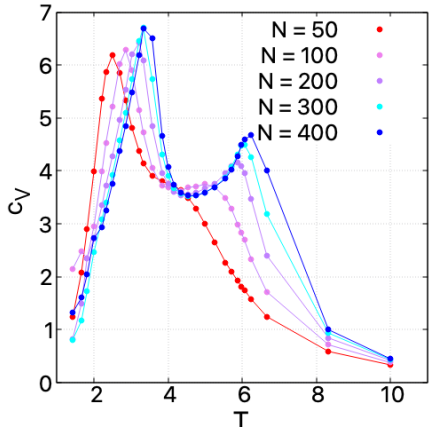

Figure 4.11: $K/J = 3$ and $\Delta = 0$. Specific heat vs temperature.

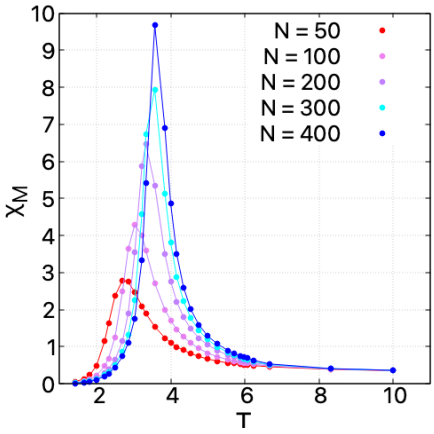

Figure 4.12: $K/J = 3$ and $\Delta = 0$. Magnetic susceptibility for different values of the temperature.

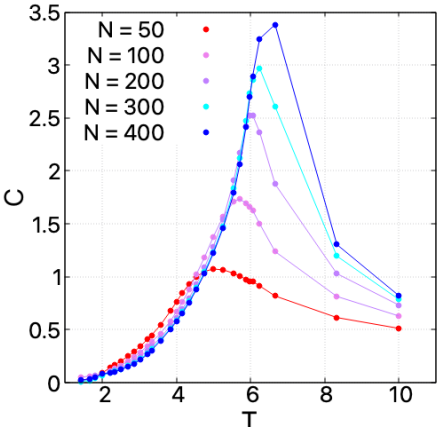

Figure 4.13: $K/J = 3$ and $\Delta = 0$. Variance of the number of contacts for different values of the temperature.

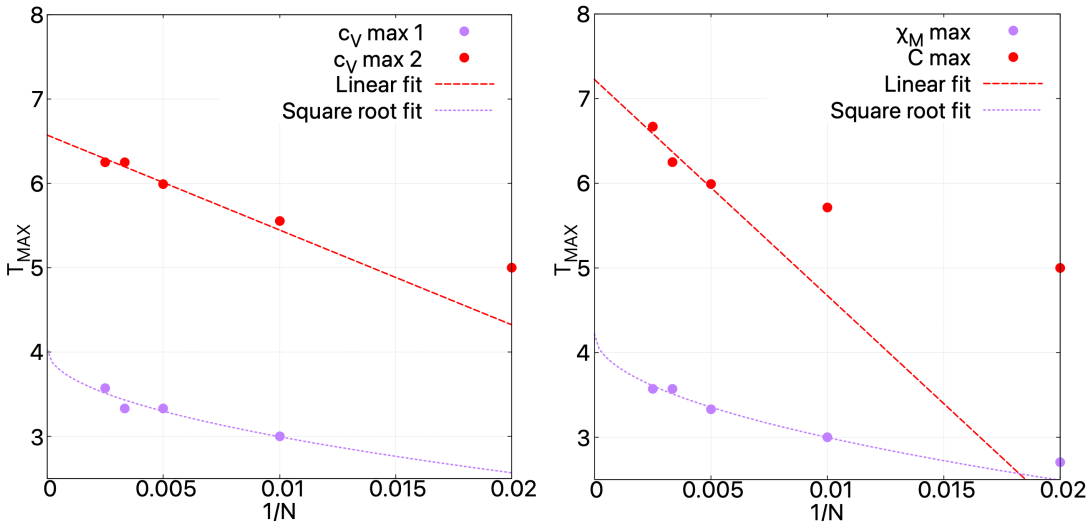

(a) (b)

Figure 4.14: $K/J = 3$ and $\Delta = 0$ and $N = 400$. (a): Temperature of the maximum of the specific heat for different N vs $1/N$. Interpolations are represented with dashed lines. (b): Temperatures of the maximum of the magnetic susceptibility and of the variance of contacts vs $1/N$. Interpolations are represented with dashed lines.

In Figures 4.14(a) and 4.14(b) two scaling analysis coming from the maximum of the specific heat (the former) for different N and from the maximum of χ_M and C for different N are shown. Since the CO - CD transition is expected to be continuous and not of first order, the shift ΔT of the critical temperature from its $N = \infty$ value is expected to go as $\sim N^{-1/2}$ (see Ref. [4]), therefore we have interpolated the first three purple points ($N = 200, 300, 400$ to avoid finite size effects) with a function of this kind. A linear fit has instead been performed for the orange points (for $N = 200, 300, 400$) because the CD - SD transition is expected to be of the first order. Again, the estimated transition temperatures seem to be lower than their mean field values.

Conclusions

In this thesis we have extended previous investigations on magnetic polymers by studying a model in which the magnetic interactions are ruled by a Blume-Emery-Griffith Hamiltonian. After having introduced the notion of a magnetic polymer (Chapter 1) and the standard Blume-Emery-Griffiths model on lattice (Chapter 2), we have computed the free energy density and the phase diagrams in the mean field approximation (Chapter 3). By varying the ratio between the strength of the biquadratic interaction K and the ferromagnetic exchange energy J, we can appreciate the richness of such phase diagrams:

- For $K/J = 0$ a first order phase transition between a swollen disordered (SD) and a compact ordered (CO) phase is predicted;
- When $K/J = 0.8$ a compact disordered (CD) phase appears. Notably, this phase was not present at equilibrium in previous studies but is expected in model of chromatin organization;
- Increasing again the ratio up to $K/J = 1.8$, a coexistence between all these three phases (CO-CD-SD) appears (i.e. a triple point); Moreover, a tricritical point in the compact-swollen phase transition is observed;
- When $K/J = 2.88$, the CO-CD transition becomes continuous;
- Finally, increasing again this ratio, the ordered phase disappears.

Numerical results based on Monte Carlo simulations (Chapter 4) of a 3D BEG polymer on a cubic lattice agree very well with the mean field predictions when $K = 0$ and $\Delta = 0, 1$, in fact the observed transition temperature between the SD and the CO phase corresponds to the mean field value. Analyzing the peaks of the specific heat, the magnetic susceptibility and of the variance of contacts, we have observed in the $K/J = 2$ and $K/J = 3$ cases, both the CO-CD and the CD-SD phase transitions, as predicted by the mean field phase diagrams.
Possible natural extensions of this thesis project are the following:

- Study magnetic models on different substrates. The polymers that we have considered here are linear polymers modeled as self avoiding walks on lattice. However the majority of natural and synthetic polymers are branched polymers, with multiple side chains attached to a main backbone one. For instance in chromatin loop extruding factors can create structures resembling bottle-brush polymers with looped side chains (see Figure 4.15). Moreover, magnetic models on higher dimensional substrates like membranes (see Figure 4.15) could be interesting for technological applications (by tuning an external magnetic field or the temperature of the system, it is possible to induce a mechanical transformation of such an object that could be exploited in ICT);

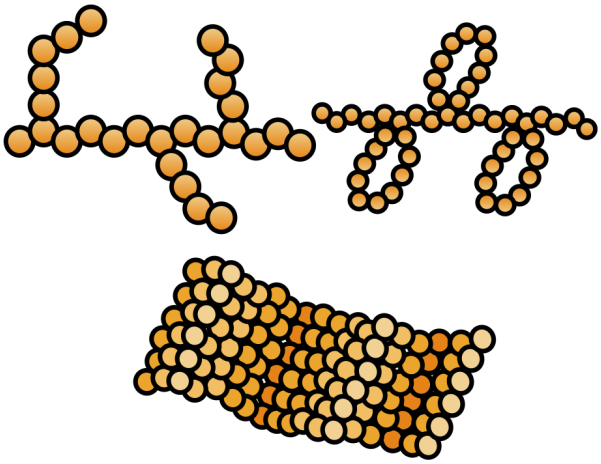

Figure 4.15: Examples of potential substrates over which one can implement magnetic-like interactions. Above there are two branched polymers, made of side chains attached to a main backbone chain. Below, a 2D polymer, i.e. a flexible membrane, is shown.

- Consider a bunch of several magnetically interacting polymer chains (i.e. with inter-polymer interaction terms in the Hamiltonian) as models to study, for example, the mixed-segregated phase transition, with applications to the chromosomal territories in the cell nucleus;

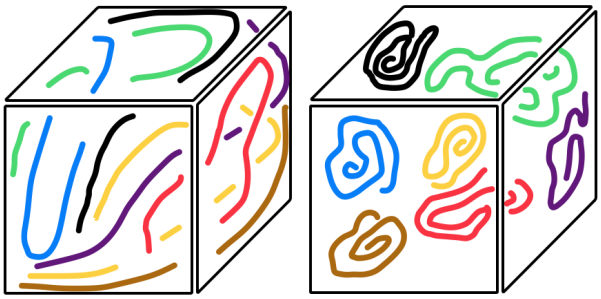

Figure 4.16: In a system of mutually interacting polymers it is possible to observe the mixed - segregated phase transition. In the mixed phase (left), polymers are intertwined with each other; in the segregated phase polymers are no more mixed and are clearly identificable.

- Going out-of-equilibrium, it could be interested to study magnetic models on active polymers, i.e. whose monomers consume internal or environmental energy in order to move. Chromatin itself is an out-of-equilibrium system because of the presence of enzymes and molecular motors running on the DNA filament thanks to the hydrolysis of ATP.

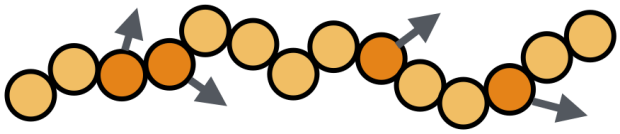

Figure 4.17: In an active polymer, some monomers exploit internal or environmental energy in order to move. In this picture active monomers are colored in orange and a grey arrows indicate their velocity.

Appendix A

Analytical calculations

A.1 Analytical derivation of the mean field free energy for an Ising magnetic polymer

In this section, we derive the mean field free energy of an Ising magnetic polymer. Let us start from the partition function of this system

$$\mathcal{Z} = \sum_{\gamma \in \mathrm{SAW}} \sum_{\{S\}} \exp\left(\frac{\beta J}{2} \sum_{i,j} S_i \Lambda^{\gamma}_{i,j} S_j + \beta h \sum_i S_i\right) =$$

$$= \sum_{\gamma \in \mathrm{SAW}} \sum_{\{S\}} \exp\left(\frac{\beta J}{2} \sum_{i,j} S_i \Lambda^{\gamma}_{i,j} S_j\right) \exp\left(\beta h \sum_i S_i\right). \tag{A.1}$$

It is difficult to perform the double summation in the first term on the rhs of Eq. (A.1) because of the presence of two different spins in the factor inside the blue box. Therefore it is worth to perform an Hubbard - Stratonovich transformation to decouple them by introducing additional field variables. Given a matrix $\hat{A} \in \mathbb{R}^{n \times n}$ and a vector $\mathbf{b} \in \mathbb{R}^n$ the Hubbard - Stratonovich transformation can be written as:

$$\int d^N x \exp\left(-\frac{1}{2} \sum_{ij} x_i A_{ij} x_j + \sum_i b_i x_i\right) = (2\pi)^{N/2} (\det A)^{-1/2} \exp\left(\frac{1}{2} \sum_{i,j} b_i A^{-1}_{ij} b_j\right) \tag{A.2}$$

Therefore by applying the following substitutions:

$$b_i = S_i \tag{A.3}$$

$$b_j = S_j \tag{A.4}$$

$$A_{ij} = \beta J \Lambda_{i,j} \tag{A.5}$$

we can write:

$$\det A = (\beta J)^{-N} \det((\Lambda^{\gamma})^{-1}) = (\beta J)^{-N} \det(\Lambda^{\gamma})^{-1} \tag{A.6}$$

(we assumed $\hat{\Lambda}$ is an invertible matrix) and so the term inside the box can be rewritten as:

$$\exp\left(\frac{\beta J}{2}\sum_{i,j} S_i \Lambda^{\gamma}_{i,j} S_j\right) = \tag{A.7}$$

$$= (2\pi)^{-N/2}(\beta J)^{-N/2}\det(\Lambda)^{-1/2}\cdot\int d^N\phi \exp\left(-\frac{1}{2\beta J}\sum_{i,j}\phi_i(\Lambda^{\gamma}_{i,j})^{-1}\phi_j + \sum_i S_i\phi_i\right) \tag{A.8}$$

where $d^N\phi \equiv \prod_{i=1}^N d\phi_i$. Let us call:

$$D\phi \equiv (2\pi)^{-N/2}(\beta J)^{-N/2}\det(\Lambda)^{-1/2} d^N\phi. \tag{A.9}$$

Thus, continuing the chain of equivalences:

$$= \int D\phi \exp\left(-\frac{1}{2\beta J}\sum_{i,j}\phi_i(\Lambda^{\gamma}_{i,j})^{-1}\phi_j + \sum_i S_i\phi_i\right). \tag{A.10}$$

Plugging this result in Eq. (A.1):

$$\mathcal{Z} = \sum_{\gamma\in \mathrm{SAW}}\sum_{\{S\}}\int D\phi \exp\left(-\frac{1}{2\beta J}\sum_{i,j}\phi_i(\Lambda^{\gamma}_{i,j})^{-1}\phi_j + \sum_i S_i(\phi_i+\beta h)\right) = \tag{A.11}$$

$$= \sum_{\gamma\in \mathrm{SAW}}\int D\phi \exp\left(-\frac{1}{2\beta J}\sum_{i,j}\phi_i(\Lambda^{\gamma}_{i,j})^{-1}\phi_j\right) \boxed{\sum_{\{S\}}\prod_{i=1}^N \exp\left(S_i(\phi_i+\beta h)\right)} \tag{A.12}$$

The expression in the box can be easily summated:

$$\sum_{\{S\}}\prod_{i=1}^N \exp\left(S_i(\phi_i+\beta h)\right) = \prod_{i=1}^N\sum_{S_i\in\{\pm 1\}} \exp\left(S_i(\phi_i+\beta h)\right) = \tag{A.13}$$

$$= \prod_{i=1}^N 2\cosh(\phi_i+\beta h) = \tag{A.14}$$

$$= \exp\left(\sum_{i=1}^N \log(2\cosh(\phi_i+\beta h))\right). \tag{A.15}$$

where some elementary steps have been performed. Plugging it in place of the old expression inside the box we find:

$$\mathcal{Z} = \sum_{\gamma\in \mathrm{SAW}}\int D\phi \exp\left(-\frac{1}{2\beta J}\sum_{i,j}\phi_i(\Lambda^{\gamma}_{i,j})^{-1}\phi_j + \sum_{i=1}^N \log(2\cosh(\phi_i+\beta h))\right) \tag{A.16}$$

A mean field theory is achieved following the steepest descent approximation (or homogeneous saddle point approximation) i.e. by replacing the integral with the value of the integrand at its maximum which we assume is attained for $\phi_i = \phi$ for all i (see Refs. [3], [4], [6]):

$$\mathcal{Z} \approx A\sum_{\gamma\in \mathrm{SAW}} \exp\left(-\frac{\phi^2}{2\beta J}\sum_{i,j}(\Lambda^{\gamma}_{i,j})^{-1} + N\log\cosh(\phi+\beta h)\right) \tag{A.17}$$

where A is a constant. Using the Hamiltonian walks restriction, as reported in Chapter 1,

$$\sum_{i,j}(\Lambda^{\gamma}_{i,j})^{-1} \approx \frac{N}{\rho z}. \tag{A.18}$$

Plugging this result in Eq. (A.17) we obtain:

$$\mathcal{Z} \approx A \sum_{\gamma \in \mathrm{SAW}} \exp\left(-\frac{N\phi^2}{2\beta\rho z J} + N\log(2\cosh(\phi+\beta h))\right). \tag{A.19}$$

As a last step, since the specific walk γ does not appear anymore, we need an estimation the number of SAWs of $N-1$ steps on a lattice of volume V. As shown in Ref. [4]:

$$\mathcal{Z}_{SAW} = \sum_{\gamma \in SAW} 1 = \left(\frac{z}{e}\right)^N \exp\left(-V(1-\rho)\log(1-\rho)\right). \tag{A.20}$$

Finally, the mean field partition function is:

$$\mathcal{Z} \approx A\left(\frac{z}{e}\right)^N \exp\left(-V(1-\rho)\log(1-\rho) - \frac{N\phi^2}{2\beta\rho z J} + \log(2\cosh(\phi+\beta h))\right), \tag{A.21}$$

and the mean field free energy density of this model is:

$$f(\phi,\rho,\beta;J,h) = +\frac{\phi^2}{2\rho\beta^2 J z} - \frac{1}{\beta}\log\frac{z}{e} + \frac{1}{\beta}\frac{1-\rho}{\rho}\log(1-\rho) - \frac{1}{\beta}\log(2\cosh(\phi+\beta h)). \tag{A.22}$$

A.2 Analytical derivation of the mean field free energy for the lattice BEG model

The approach followed in this Appendix is the same of the previous one. However there are important differences:

- This model is defined on a lattice, therefore the matrix Λ is the adjacency matrix of the lattice. In particular, the following identity holds:

$$\sum_{i,j}(\Lambda_{i,j})^{-1} = \frac{N}{z} \tag{A.23}$$

- Because of the presence of a biquadratic term in the Hamiltonian an additional Hubbard-Stratonovich transformation is needed, with the consequent appearance of a new set of fields $\{\alpha_i\}$. After this transformation, the partition function becomes:

$$\mathcal{Z} = \sum_{\{S\}}\int D\phi D\alpha \tag{A.24}$$

$$\exp\left(-\frac{1}{2\beta J}\sum_{i,j}\phi_i\Lambda_{i,j}\phi_j - \frac{1}{2\beta K}\sum_{i,j}\alpha_i\Lambda_{i,j}\alpha_j + \sum_i(\phi_i S_i + \alpha_i S_i^2 - \beta\Delta S_i^2) + \beta\Delta N\right), \tag{A.25}$$

where

$$D\alpha \equiv (2\pi)^{-N/2}(\beta K)^{-N/2}\det(\Lambda)^{-1/2}d^N\alpha. \tag{A.26}$$

- The spin variables can assume three values: $0, \pm 1$ and in the final free energy expression this fact will affect terms related to hyperbolic functions. We can easily expand the summation on the spin variables:

$$\sum_{\{S\}} \prod_{i=1}^{N} \exp\left(\phi_i S_i + \alpha_i S_i^2 - \beta\Delta S_i^2\right) = \prod_{i=1}^{N} \sum_{S_i=0,\pm 1} \exp\left(\phi_i S_i + \alpha_i S_i^2 - \beta\Delta S_i^2\right) \tag{A.27}$$

$$= \prod_{i=1}^{N} (1 + 2e^{-\beta\Delta+\alpha_i}\cosh(\phi_i)) \tag{A.28}$$

$$= \exp\left(\sum_{i=1}^{N} \log(1 + 2e^{-\beta\Delta+\alpha_i}\cosh(\phi_i))\right). \tag{A.29}$$

After these steps we get:

$$\mathcal{Z} = A \int D\phi D\alpha \tag{A.30}$$

$$\exp\left(-\frac{1}{2\beta J}\sum_{i,j}\phi_i(\Lambda_{i,j})^{-1}\phi_j - \frac{1}{2\beta K}\sum_{i,j}\alpha_i(\Lambda_{i,j})^{-1}\alpha_j + \sum_{i=1}^{N}\log(1 + 2e^{-\beta\Delta+\alpha_i}\cosh(\phi_i))\right) \tag{A.31}$$

Eventually, after an homogeneous saddle point approximation and using Eq. (A.23) we obtain the expressions for the mean field partition function and the mean field free energy density:

$$\mathcal{Z} = A\left(\frac{z}{e}\right)^N \exp\left(-\frac{N\phi^2}{2\beta z J} - \frac{N\alpha^2}{2\beta z K} + N\log(1 + 2e^{-\beta\Delta+\alpha}\cosh(\phi))\right), \tag{A.32}$$

$$f(\beta,\phi,\alpha,\rho) = \frac{1}{2\beta^2 z}\left(\frac{\phi^2}{J} + \frac{\alpha^2}{K}\right) - \frac{1}{\beta}\log(1 + 2e^{-\beta\Delta+\alpha}\cosh(\phi)) - \Delta. \tag{A.33}$$

where ϕ and α minimize the exponent of Eq. (A.31).
If we do not include the biquadratic interaction term ($K = 0$) in the Hamiltonian, the mean field partition function and the mean field free energy density become:

$$\mathcal{Z} = \exp\left(-\frac{N\phi^2}{2z\beta J} + N\log\left(1 + 2e^{-\beta\Delta}\cosh(\phi)\right) + \beta\Delta N\right), \tag{A.34}$$

$$f(\phi,\beta,\Delta) = \frac{\phi^2}{2z\beta^2 J} - \frac{1}{\beta}\log\left(1 + 2e^{-\beta\Delta}\cosh(\phi)\right) - \Delta. \tag{A.35}$$

If instead we do not include the ferromagnetic interaction term in the Hamiltonian, we find:

$$\mathcal{Z} = A\left(\frac{z}{e}\right)^N \exp\left(-\frac{N\alpha^2}{2\beta z K} + N\log(1 + 2e^{-\beta\Delta+\alpha})\right), \tag{A.36}$$

$$f(\beta,\alpha,\rho) = \frac{1}{2\beta^2 z}\frac{\alpha^2}{K} - \frac{1}{\beta}\log(1 + 2e^{-\beta\Delta+\alpha}) - \Delta. \tag{A.37}$$

A.3 BEG model free energy expansion (no biquadratic interaction)

In this section we perform the Taylor expansion of the free energy density when there is no biquadratic interaction. Looking at the coefficients of the expansion it is possible to find critical

and tricritical points.
In order to study the critical properties of this model we want to Taylor expand the free energy density Eq. (A.35). Because of the $\mathbb{Z}_2$ symmetry of this model we expect to observe only even powers of ϕ in the Taylor expansion of $f(\phi, \beta, \Delta)$ around $\phi = 0$.
We need the Taylor expansions of the logarithm and of the hyperbolic cosine:

$$\log(1+x) = x - \frac{x^2}{2} + \dots \tag{A.38}$$

$$\cosh x = 1 + \frac{x^2}{2!} + \frac{x^4}{4!} + \dots \tag{A.39}$$

Proceeding with the expansion of the hyperbolic cosine inside the logarithm:

$$\begin{aligned}
\log(1 + 2e^{-\beta\Delta}\cosh\phi) &\approx \log\left(1 + 2e^{-\beta\Delta}\left(1 + \frac{\phi^2}{2!} + \frac{\phi^4}{4!}\right)\right) \\
&= \log\left(1 + 2e^{-\beta\Delta} + 2e^{-\beta\Delta}\left(\frac{\phi^2}{2!} + \frac{\phi^4}{4!}\right)\right) \\
&= \log\left(1 + 2e^{-\beta\Delta}\right) + \log\left(1 + \frac{2e^{-\beta\Delta}}{1 + 2e^{-\beta\Delta}}\left(\frac{\phi^2}{2!} + \frac{\phi^4}{4!}\right)\right) \\
&= \log\left(\frac{\delta}{\delta - 1}\right) + \boxed{\log\left(1 + \frac{1}{\delta}\left(\frac{\phi^2}{2!} + \frac{\phi^4}{4!}\right)\right)}
\end{aligned} \tag{A.40}$$

where we have defined:

$$\delta(\beta, \Delta) \equiv \frac{1 + 2e^{-\beta\Delta}}{2e^{-\beta\Delta}} = 1 + \frac{e^{\beta\Delta}}{2} \tag{A.41}$$

Now we can proceed expanding the logarithm inside the box up to the sixth order on ϕ:

$$\log\left(1 + \frac{1}{\delta}\left(\frac{\phi^2}{2!} + \frac{\phi^4}{4!}\right)\right) \approx \frac{1}{\delta}\left(\frac{\phi^2}{2!} + \frac{\phi^4}{4!}\right) - \frac{1}{\delta^2}\left(\frac{\phi^4}{8} + \frac{\phi^6}{48}\right) \tag{A.42}$$

We get finally:

$$\log(1 + 2\exp(-\beta\Delta)\cosh(\phi) \approx \log\left(\frac{\delta}{\delta - 1}\right) + \frac{1}{2\delta}\phi^2 + \frac{1}{8}\left(\frac{1}{3\delta} - \frac{1}{\delta^2}\right)\phi^4 - \frac{1}{48\delta^2}\phi^6 \tag{A.43}$$

and the free energy expansions in terms of ϕ is (neglecting terms that do not depend on ϕ):

$$\begin{aligned}
f(\beta, \Delta) &= \left(\frac{1}{2\beta^2 Jz} - \frac{1}{2\beta\delta}\right)\phi^2 - \frac{1}{8\beta}\left(\frac{1}{3\delta} - \frac{1}{\delta^2}\right)\phi^4 + \frac{1}{48\beta\delta^2}\phi^6 \\
&= a(\beta, \Delta)\phi^2 + b(\beta, \Delta)\phi^4 + c(\beta, \Delta)\phi^6
\end{aligned} \tag{A.44}$$

where we have defined:

$$a(\beta, \Delta) = \left(\frac{1}{2\beta^2 Jz} - \frac{1}{2\beta\delta}\right) \tag{A.45}$$

$$b(\beta, \Delta) = -\frac{1}{8\beta}\left(\frac{1}{3\delta} - \frac{1}{\delta^2}\right) \tag{A.46}$$

$$c(\beta, \Delta) = \frac{1}{48\beta\delta^2} \tag{A.47}$$

Notice that $c(\beta, \Delta) > 0$ while instead $a(\beta, \rho, \Delta)$ and $b(\beta, \Delta)$ may change sign.

A.4 Analytical derivation of the mean field free energy for the lattice polymer BEG model

In the case of the BEG magnetic polymer we can compute the free energy density exactly as in section 2 but replacing identity Eq. (A.23) with the identity Eq. (A.18) and remembering to add a summation on all the SAWs of length N in a volume V in the computation of the partition function. The mean field partition function and the mean field free energy density are in the end:

$$\mathcal{Z} \approx A \exp\left(N \log \frac{z}{e} - \frac{1-\rho}{\rho} \log(1-\rho) - \frac{\phi^2 N}{2\beta J z \rho} - \frac{\alpha^2 N}{2\beta K z \rho} + N \log(1 + 2e^{-\beta\Delta+\alpha} \cosh\phi) + \beta\Delta N \right) \tag{A.48}$$

$$f(\beta,\rho,\Delta) = -\frac{1}{\beta}\log\frac{z}{e} + \frac{1}{\beta}\frac{1-\rho}{\rho}\log(1-\rho) + \frac{\phi^2}{2\beta^2 J z\rho} + \frac{\alpha^2}{2\beta^2 K z\rho} - \frac{1}{\beta}\log\left(1 + 2e^{-\beta\Delta+\alpha}\cosh\phi\right) - \Delta \tag{A.49}$$

A.5 BEG magnetic polymer at fixed polymer density

How the critical properties of a BEG polymer change when the polymer density ρ is fixed? Let us consider the $K = 0$ case, i.e. without the biquadratic interaction. Since ρ is a fixed parameter, the Taylor expansion of the free energy density around $\phi = 0$ is formally identical to Eq. (A.44): the only difference is the presence of ρ in the coefficient in front of ϕ^2:

$$\begin{aligned} f(\beta,\rho,\Delta) &= \left(\frac{1}{2\beta^2 J z\rho} - \frac{1}{2\beta\delta}\right)\phi^2 - \frac{1}{8\beta}\left(\frac{1}{3\delta} - \frac{1}{\delta^2}\right)\phi^4 + \frac{1}{48\beta\delta^2}\phi^6 \\ &= a(\beta,\rho,\Delta)\phi^2 + b(\beta,\Delta)\phi^4 + c(\beta,\Delta)\phi^6 \end{aligned}$$

where we have defined:

$$a(\beta,\rho,\Delta) = \left(\frac{1}{2\beta^2 J z\rho} - \frac{1}{2\beta\delta}\right) \tag{A.50}$$

$$b(\beta,\Delta) = -\frac{1}{8\beta}\left(\frac{1}{3\delta} - \frac{1}{\delta^2}\right) \tag{A.51}$$

$$c(\beta,\Delta) = \frac{1}{48\beta\delta^2} \tag{A.52}$$

As expected the coefficient of the sixth power, is always positive: $c(\beta,\Delta) > 0$.
The critical temperature in terms of the polymer concentration ρ and the parameter Δ can be estimated by solving $a(\beta,\rho,\Delta) = 0$ with respect to β. First notice how the concentration of vacancies in the disordered phase ($\phi = 0$) is related to the parameter δ:

$$x(\phi=0) = \frac{1}{1+2e^{-\beta\Delta}} = \frac{\delta-1}{\delta}$$

which implies:

$$\delta = \frac{1}{1-x(\phi=0)}$$

Thus the critical temperature can be obtained as:

$$\beta_c = \frac{\delta}{Jz\rho} \to T_c(x) = \frac{Jz\rho}{k_B}(1-x(\phi=0))$$

which displays a linear dependence on the concentration of vacancies. This results is very similar to the BEG on the lattice: the only difference is the direct proportionality with respect to the polymer concentration ρ which affects the slope of the line in the $T - x$ plane.
The tricritical point is obtained as usual:

$$\begin{aligned} a(\beta, \rho, \Delta) &= 0 \\ b(\beta, \Delta) &= 0 \end{aligned}$$

The second equation implies $\delta_{tc} = 3$, $x = 2/3$ and therefore:

$$T_{tc} = \frac{Jz\rho}{3k_B}$$

This point separate continuous phase transitions from first oder ones. Again, the only difference with respect to the squared lattice situation is that $T_{tc} \propto \rho$.

A.6 BEG model and offset

In this section we reproduce the results of the Ref. [6] They show that, when an overall attractive term is added in the Hamiltonian of the system, a CD phase appears in the mean field phase diagram for certain values of the parameters. The same notation of the previous sections holds.
For simplicity we illustrate the case where $K = 0$. Given two spins S_i, S_j belonging to the i-th and j-th monomers of the polymer, the ferromagnetic interaction can be parametrized as:

$$I(S_i, S_j) = -JS_iS_j - 2c \tag{A.53}$$

where $J > 0$ is the ferromagnetic coupling and $c > 0$ is an offset parameter. When $c = 0$ we come back to the standard BEG hamiltonian.

$$\mathcal{H}_c \approx \frac{1}{2}\sum_{i,j} I(S_i, S_j)\Lambda_{i,j} + \Delta\sum_{i=1}^{N} S_i^2 - \Delta N \tag{A.54}$$

In order to derive the partition function and then the mean field free energy per monomer the same procedure followed in the other cases is applied. The main difference is the presence of the following contribution inside the Boltzmann factors:

$$\beta c\sum_{i,j}\Lambda_{i,j} = \beta cN\rho z \tag{A.55}$$

which is involved neither in the Hubbard-Stratonovich transformation nor in the summation on the spin variables. The free energy per monomer is:

$$f_c(\phi, \rho; \beta, \Delta) = f(\phi, \rho; \beta, \Delta) - cz\rho \tag{A.56}$$

$$= -\frac{1}{\beta}\log\frac{z}{e} + \frac{1}{\beta}\frac{1-\rho}{\rho}\log(1-\rho) + \frac{\phi^2}{2\beta^2 Jz\rho} - \frac{1}{\beta}\log\left(1 + 2e^{-\beta\Delta}\cosh\phi\right) - \Delta - cz\rho \tag{A.57}$$

In order to understand the critical properties of such a model we make use of the virial expansion.

A.6.1 CD - SD phase transition

Since we are looking for a transition between two disordered phase, we can plug $\phi = 0$ in the expression of the free energy, compute the osmotic pressure $\Pi(\rho)$ and Taylor expand it around $\rho = 0$:

$$\frac{\beta\Pi}{\rho} = \left(\frac{1}{2} - cz\beta\right)\rho + \frac{\rho^2}{3} + \frac{\rho^3}{4} + \frac{\rho^4}{5} + \dots \tag{A.58}$$

The second virial coefficient is therefore:

$$B_2(T) = \frac{1}{2} - cz\beta \tag{A.59}$$

And the others are:

$$B_j(T) = 1/j \tag{A.60}$$

where $j > 2$. A continuous phase transition between the two phases occurs when:

$$T = 2zc \tag{A.61}$$

which is independent on the typical quantities of the BEG model.

A.6.2 CO - CD phase transition

We are now interested in studying the transition between two compact phases, an ordered and a disordered one. Let us consider the mean field equations:

$$\frac{\phi}{\beta z J \rho} = \frac{\sinh\phi}{\cosh\phi + \frac{e^{\beta\Delta}}{2}} \tag{A.62}$$

$$czJ\beta\rho^2 + \rho + \frac{\phi^2}{2zJ\beta} + \log(1-\rho) = 0 \tag{A.63}$$

Notice how the offset parameter c appears only in the second equation. Both the CO and the CD phases are characterized by a finite and positive polymer concentration $\rho > 0$ while instead $\phi > 0$ in the CO phase and $\phi \approx 0$ in the CD phase.
Expanding the first equation up to the third order we can derive an estimation of the field ϕ:

$$\phi^2 \approx \frac{6(\beta z J\rho - \delta)}{\frac{3\beta z J\rho}{\delta} - z\beta J\rho} \tag{A.64}$$

In order to study the CO - CD transition we should expand the free energy for small ϕ which is equivalent to plug Eq. (A.64) in the free energy density Eq. (A.57) and expand it around $\rho^* = \delta/(\beta z J)$ (the value of the polymer density such that $\phi(\rho^*) = 0$). In this way we obtain a virial like expansion:

$$\frac{\beta\Pi}{(\rho - \rho^*)} = B_2(T,c)(\rho-\rho^*) + B_3(T)(\rho-\rho^*)^2 + B_4(T)(\rho-\rho^*)^3 + \dots \tag{A.65}$$

Where the expression of the second and third virial coefficients are respectively:

$$B_2(T,\delta,c) = -\frac{z\left(c\delta^2 + \delta + \beta z\log\left(1 - \frac{\delta}{\beta z}\right)\right)}{\delta^2} \tag{A.66}$$

$$B_3(T,\delta) = \frac{3\beta z^2\left(2\beta z\log\left(1-\frac{\delta}{\beta z}\right) - \frac{\delta\left(\delta^2+\beta(3-2\delta)z\right)}{(\delta-3)(\beta z-\delta)}\right)}{2\delta^3} \tag{A.67}$$

Notice that offset parameter c enters only in the B_2 coefficient and not in the higher order virial coefficients. Moreover, because of the expansion of the $(1-\rho)/\rho \log(1-\rho)$ term of the free energy, a logarithm appears in the previous two coefficient, forcing the ratio $\delta/(\beta z)$ to be greater than one:

$$\frac{\delta}{\beta z} > 1 \quad \text{or equivalently} \quad x(\phi = 0) < 1 - \frac{T}{z} \tag{A.68}$$

Which coincides interestingly with the critical condition of the lattice BEG model (valid again only if $\delta < 3$). The physical meaning is the following:

- When $c < 0.6$ only discontinuous transitions from the CO to the CD phases can occur. This corroborates further the discontinuous transition observed in the non - offset model case $c = 0$;
- When $c = 0.6$ a special situation occurs: two lines of first order phase transitions bifurcate where both the second and the third virial coefficients vanish (see Figure A.1(b));
- When $0.6 < c < 0.9$ a line of critical points is between two lines of first order phase transitions between the CO and the CD phases. Therefore there exists two tricritical points;
- If $c > 0.9$ only one of the two tricritical point survives and when $c \to \infty$ this point tends to the tricritical point of the lattice BEG model. In fact one can show that in this limit both the virial coefficients vanish at (x_{TC}, T_{TC}).

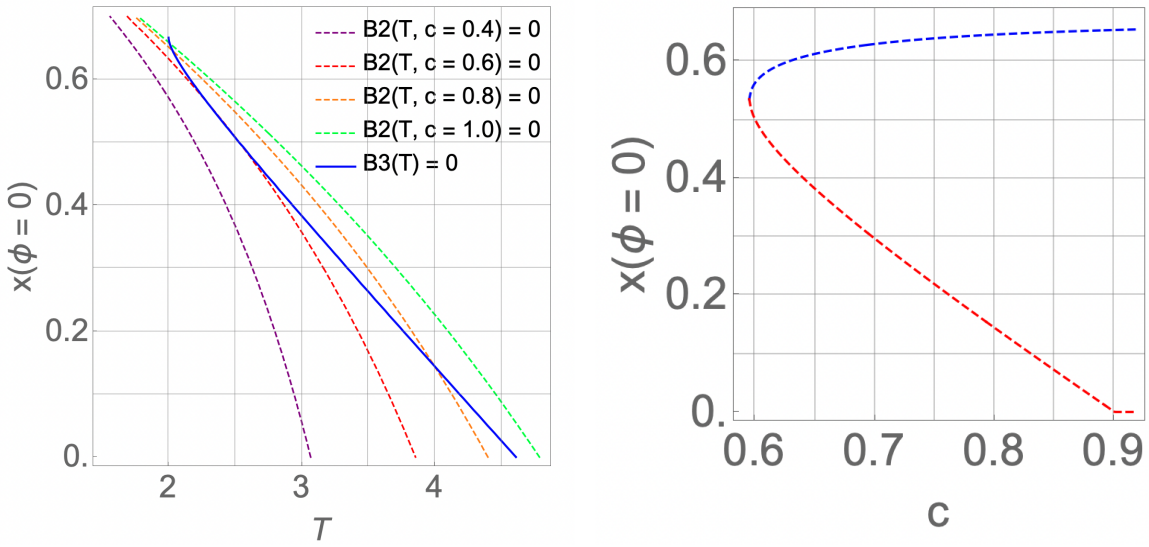

(a) (b)

Figure A.1: (a): curves corresponding to the vanishing of the second and third virial coefficients. Since B_3 does not depend on c, the condition $B_3(T, \delta) = 0$ is represented by a unique line. The $B_2(T, \delta, c) = 0$ is shown for four different values of the offset parameter. (b): how the coordinate $x(\phi = 0)$ of the tricritical points changes by varying the offset. One of the two tends to the tricritical point of the lattice BEG model. The other one vanishes at 0 temperature around $c \approx 0.9$.

Bibliography

[1] M. Rubinstein and R. H. Colby. *Polymer Physics*. New York: Oxford University Press, 2003.

[2] Jean-Pierre Hansen and I.R. McDonald. *Theory of simple liquids*. 4th ed. 2013.

[3] Davide Coli et al. "Magnetic polymer models for epigenetics-driven chromosome folding". In: *Phys. Rev. E* 100 (5 Nov. 2019), p. 052410. DOI: 10.1103/PhysRevE.100.052410.

[4] Thomas Garel, H. Orland, and Enzo Orlandini. "Phase diagram of magnetic polymers". In: *The European Physical Journal B* 12 (Feb. 1999). DOI: 10.1007/s100510051003.

[5] M. Blume, V. J. Emery, and Robert B. Griffiths. "Ising Model for the λ Transition and Phase Separation in He^3-He^4 Mixtures". In: *Phys. Rev. A* 4 (3 Sept. 1971), pp. 1071–1077. DOI: 10.1103/PhysRevA.4.1071.

[6] Ryo Nakanishi and Koji Hukushima. "Emergence of compact disordered phase in a polymer Potts model". In: *Phys. Rev. E* 109 (1 Jan. 2024), p. 014405. DOI: 10.1103/PhysRevE.109.014405.

[7] Andrea Papale and Angelo Rosa. "The Ising model in swollen vs. compact polymers: Mean-field approach and computer simulations." eng. In: *Eur Phys J E Soft Matter* 41.12 (Dec. 2018), p. 144. ISSN: 1292-895X (Electronic); 1292-8941 (Linking). DOI: 10.1140/epje/i2018-11752-2.

[8] Ruggero Cortini et al. "The physics of epigenetics". In: *Rev. Mod. Phys.* 88 (2 Apr. 2016), p. 025002. DOI: 10.1103/RevModPhys.88.025002. URL: https://link.aps.org/doi/10.1103/RevModPhys.88.025002.

[9] Tesi M. C. et al. "Monte Carlo Study of the Interacting Self-Avoiding Walk Model in Three Dimensions". In: *Journal of Statistical Physics,* 82 (1996), pp. 155–181.

[10] Davide Coli. "Magnetic Polymer Models for Epigenomic Spreading and Chromatin Organization". In: *Research Padua archive,* (2020).